

Rochester Institute of Technology

RIT Digital Institutional Repository

Theses

7-28-2010

Optimization of the purification and processing of carbon nanotubes for strong, conductive and lightweight wires

Brian Moses

Follow this and additional works at: <https://repository.rit.edu/theses>

Recommended Citation

Moses, Brian, "Optimization of the purification and processing of carbon nanotubes for strong, conductive and lightweight wires" (2010). Thesis. Rochester Institute of Technology. Accessed from

This Thesis is brought to you for free and open access by the RIT Libraries. For more information, please contact repository@rit.edu.

Optimization of the Purification and Processing of Carbon Nanotubes for Strong, Conductive and Lightweight Wires

By

Brian T. Moses

A THESIS

Submitted in partial fulfillment of the requirements

for the degree of Masters of Science

in

Mechanical Engineering

of the College of Engineering

at the

Rochester Institute of Technology

July 28, 2010

Optimization of the Purification and Processing of Carbon Nanotubes for Strong, Conductive and Lightweight Wires

By

Brian T. Moses

We, the undersigned members of the Faculty of the Rochester Institute of Technology, certify that we have advised and/or supervised the candidate on the work described in this dissertation. We further certify that we have reviewed the dissertation manuscript and approve it in partial fulfillment of the requirements of the degree of Masters of Science in Mechanical Engineering.

Approved by:

Dr. Ryne P. Raffaele

Dr. Robert Stevens

Dr. Steven Weinstein

Dr. John Andersen

Dr. Steven Day

Abstract

Single walled carbon nanotubes are produced using standard synthesis and purification techniques. Bulk materials produced using filtration drying are characterized mechanically and electrically for engineering properties. Modifications to the purification process are explored with consideration given for the effects on electrical conductivity and mechanical strength. Raman spectroscopy, thermal oxidation profiling, and high-temperature vacuum annealing are used to gain further insight on the connection between defects and nanotube oxidation during the purification process. It is observed that the mechanical properties are strongly temperature dependent, while electrical conductivity varies with humidity rather than temperature. The use of a thermal vacuum anneal can improve separation of oxidative processes between nanotubes and carbon in the time domain, allowing further optimization of the thermal processing and improved physical properties of nanotube bulk materials post-processing.

Acknowledgements

I would like to thank the National Reconnaissance Office for their financial support, the Nanopower Research Labs for the opportunity to pursue this research, Dr. John Andersen for his advice and insights into science, Dr. Paul Jarosz for keeping me motivated through this daunting process, and Dr. Ryne Raffaele for his role as adviser and commitment to his students' future success.

Contents

Abstract.....	iii
Acknowledgements.....	iv
Figure List.....	vi
Chapter 1: Background.....	1
Chapter 2: Literature and Theory.....	3
Chapter 3: Characterization Techniques and Equipment.....	5
Chapter 4: Description of Research Problem.....	11
Chapter 5: Production of Carbon Nanotubes.....	14
Chapter 6: Characterization.....	15
Chapter 7: Processing Modification	
Section 1 -Thermal Oxidation.....	18
Section 2: Nanostructured Carbon.....	22
Section 3: Vacuum Anneal.....	27
Section 4: Analysis of thermal oxidation.....	30
Chapter 8: Environmental Effects	
Section 1: In Situ Humidity Effects.....	32
Section 2: Strain hardening, Flexure, Crush.....	35
Chapter 9: Discussion.....	39
Chapter 10: Conclusion.....	41
References.....	43
Appendix 1: Technology Demonstrations.....	46
Appendix 2: Electrical Conductivity Measurement Station.....	48

Figure List

Figure 1 Optical absorption peak ratio reflects purity. From [12]	3
Figure 2 Conductivity of CNTs in Literature [4,8,37-57]	4
Figure 3 Conductivity Measurement	5
Figure 4 TA Q800 Dynamic Mechanical Analyzer	8
Figure 5 YAG Laser vaporization CNT synthesis	14
Figure 6 Tensile tests of Reflux material at varied temperature	15
Figure 7: (Left) Tensile tests of CNT Materials (Right) Specific Tensile Strength of Materials.....	16
Figure 8 Conductivity of synthesized CNT Material	17
Figure 9: Purification Efficiency. From [1]	18
Figure 10 Conductivity of purified nanotubes using different oxidation recipes	18
Figure 11: TGA Thermogram of SWCNT reflux material	19
Figure 12 Isothermal Mass loss	19
Figure 13: Tensile strength lost during purification.....	20
Figure 14 Conductivity loss during oxidative purification.....	21
Figure 15: Addition of Nanostructured Carbon reduces Conductivity and tensile Strength.....	24
Figure 16: (Left) SEM Image of nylon CNT composite (Right) Nylon DMA solution penetrates CNT papers; solvent removes loosely-bound carbon.....	25
Figure 17: Tensile test of reflux CNT ribbon, before and after nylon treatment.....	26
Figure 18: Thermogram of annealed SWCNT at various ramp rates	27
Figure 19: Vacuum Annealing Chamber	27
Figure 21 (Left) D/G ratio of post-anneal oxidation recipes (Right) Spectra for 475° C samples .	28
Figure 20 SEM of Annealed CNT Material.....	28
Figure 22: Tensile strength of CNT papers after isothermal oxidation	29
Figure 23 Comparison of isothermal TGA; Annealed vs Reflux SWCNT Ribbons.	30
Figure 24 Logarithmic Derivatives, Annealed Material	31
Figure 25: (Left) Comparison of 450° C Isotherm, Reflux vs Annealed. (Right) Curve-Fitting to TGA derivatives	31
Figure 26: ESPEC Environmental Chamber	32
Figure 27: Annealing is shown to change the temperature dependence of CNT conductivity	32
Figure 28: Humidity and Thermal Cycling of CNT Wires.....	33
Figure 29: Decreasing resistance with pressure.....	35
Figure 30 CNT Ribbon, before and after 1 GPA axial pressure.....	36
Figure 31: (Left) Electrical performance under bending (Right) Stiffness cyclic bending. (Below) Experimental Setup.....	37
Figure 32 Strain Hardening of SWCNT Ribbons.....	38
Figure 33: SEM Image of pre-stressed CNT Paper	38
Figure 34: AFM Analysis of Piranha Oxidation; Courtesy of Dr. Brian Landi	39
Figure 35: Conductivity and Piranha exposure	39
Figure 36: Initial D-Band (pink) reduces after 20 minutes of oxidation.....	40

Figure 37 (Left) Contact Resistance of CNTs on Metal (Right) Contact resistance measurement setup.....	46
Figure 38 (Left) Coaxial cable with CNT center. (Right) Commercial SMA, CNT Center SMA , and CNT Shielded SMA cables.	46
Figure 39 (Above) CNT Ethernet Cable (Below) CNT ribbon bonded to photovoltaic	47
Figure 40 DC Conductivity Measurement Station	47
Figure 41 Van der Pauw Sample.....	47
Figure 42 Top-level LabVIEW Code for DC Conductivity Measurement.....	47

Chapter 1 : Introduction & Background

Electrical wiring is vital to the function of all modern equipment, from telephones and calculators to state-of-the-art military satellites. Replacing copper with a suitable replacement that is lighter and less expensive has great potential. However, the role of metal conductors is not an easy one to fill with carbon because of the vast difference in charge carrier concentrations.

When carbon vapor is grown into a carbon nanotube, properties unique to this nanostructure arise; particularly remarkable is that the mobility of electrons within a nanotube becomes nearly infinite. While the properties of individual carbon nanotubes have been well studied experimentally and theoretically[2-4], the properties that arise when many nanotubes form a bulk solid are not as well understood, and further analysis into the effects of the microstructure would provide great insight into the use of these materials for electrical applications. The complexity of this analysis is stunning; not only are there billions of separate conductors with varying length and radii, but there are a number of possible nanostructures depending on the chirality tube growth. The chiral distribution gives rise to different functional band structure, different to the point that while some nanotubes are considered metallic, others can be classified as semiconductors, all of which interact to form a bulk material[5]. Understanding how carbon nanotubes (CNT) interact is an important step to incorporating the properties of individual nanotubes into a bulk material for replacement of copper and aluminum conductors.

To date, the highest recorded conductivity of bulk single walled carbon nanotubes (SWCNT) materials is about S/m (approximately 4% that of copper), while the density of SWCNT bulk material, $650 \text{ kg}/m^3$ is 6.5% that of copper. This implies that at current conductivity levels a carbon wire of large cross-sectional area could be used to replace a copper wire of equivalent mass with a 60% increase in resistive losses. Clearly more work must be done before CNT's are a suitable

replacement for power transmission, where resistive losses are high. However, for data, shielding, and low-current applications replacement of metal conductors is already attractive. Better understanding nanotube synthesis and purification is vital to improving the engineering properties of these bulk materials.

In the body of literature surrounding carbon nanotube materials, understanding the bulk physical properties of said materials is quite lacking. Theory fails to predict the dependence of bulk conductivity on morphological parameters, interestingly the bulk conductivity varies significantly *less* than one would expect upon reading the work of Behnam or Hecht[4, 6]. While single-nanotube theory predicts ultimate mechanical strengths in the TPa range[7], researchers struggle to construct material with tensile strength approaching 0.5 GPa[8]. The work presented is focused primarily on the study of bulk SWCNT nanotubes, understanding of the electrical and mechanical properties of SWCNT bulk materials and how purification processing affects them, as well as the endurance of these properties when subjected to environmental conditions differing from STP.

Chapter 2: Literature and Theory

Purity assessment and thermal oxidation

Before any serious study in nano-particles can be performed, it is of utmost importance to characterize the physical makeup of material being studied. The basic process to go from graphite to carbon nanotubes generally involves the condensation of carbon vapor in the correct conditions, either using laser ablation, chemical vapor deposition, or high pressure CO feedstock [9-11]. Purity assessment is done using both thermogravimetric analysis as well as the UV/Vis absorption spectra[12]. Through a constructed sample set using nanotube and non-nanotube carbon, it was observed that the ratio of absorption peaks change as well (Figure 1). This absorption spectra technique allows differentiation between the nanostructured carbon and the SWCNT's, while high temperature TGA (up to 1000C) allows one to verify the levels of catalyst and graphite – these materials make up the residual[1]. Analysis using this methodology allows straightforward purity level measurements. This process is valuable to the work presented here, where the purification process is optimized for physical properties in contrast to high purity.

Tube synthesis

Much research found in literature focus on chemical vapor deposition produced carbon nanotubes. This is a high volume production method[13], however, the quality of nanotubes grown in such fashion leaves much to be desired. Much of this work focuses on material produced using graphite/catalyst laser ablation synthesis[14], specifically using the Nanopower Research Lab's (NPRL) Nd-Yag laser, three-zone furnace and standard process parameters described in Part 2. In addition to the material synthesized, some characterization is also done on sheets of SWCNT material commercially produced.

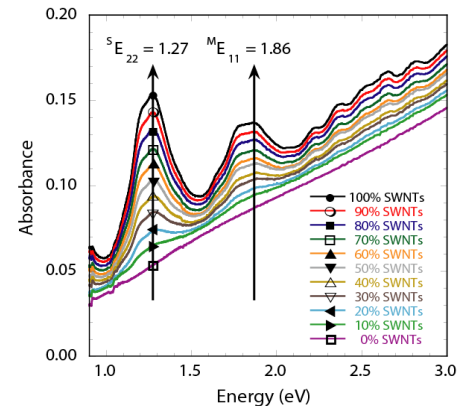


Figure 1 Optical absorption peak ratio reflects purity. From [12]

Theory behind CNT conductivity

A great deal of work has been performed by others attempting to understand how a bulk of SWCNTs conducts electricity through the matrix[15]. Current theory suggests that a pristine nanotube acts as a ballistic conductor, with the electrons tunneling from one tube to another as necessary to complete the circuit[2, 16]. This

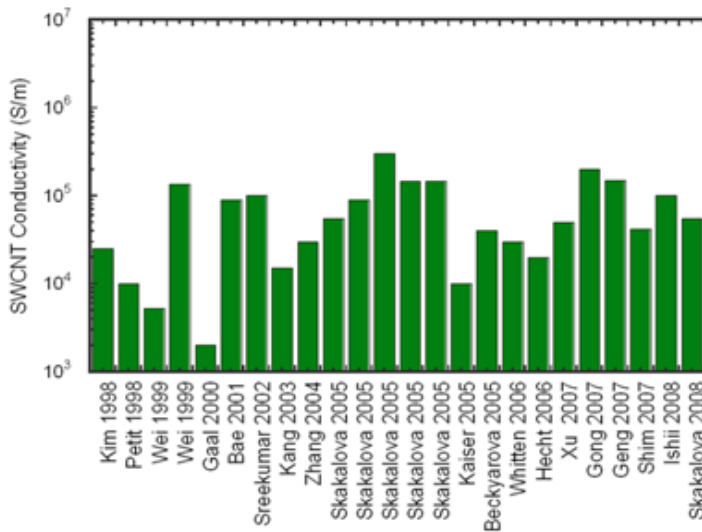


Figure 2 Conductivity of CNTs in Literature [4,8,37-57]

micro scale alignment of the nanotubes determines the number of hops necessary, while the chirality, and separation distance of any two nanotubes can modify the hopping resistance[5]. Finally, the ambient environment can interact with the tube-tube interactions, allowing chemical dopants to successfully modify the conductivity[17].

A thorough literature search for bulk ribbons consisting of single-walled carbon nanotubes highlights the variability in conductance- values range over 2 orders of magnitude. The results of this search are shown in Figure 2. Much of the successful conductivity research focuses on chemical doping, and the NPRL in particular has had great success with gold bromide, resulting in nanotube wires with conductivity of 2×10^6 S/m.

tunneling, with a significantly longer time constant, provides the bulk of any resistance measured. Additionally, defect sites located on the sidewall slow the transfer of electrons through a nanotube, resulting in a variable through-tube resistance; however defects also provide additional exit points for an electron. The length and

Chapter 3: Characterization Techniques

Raman Spectroscopy

Raman spectra are primarily used in this work for the ability to measure the D and G band signal resonance strength. Application of the technique to CNTs was pioneered by M. Dresselhaus, and has been shown to be extraordinarily effective at detecting diameter changes and defects in SWCNT materials[18, 19]. This technique gives the crystalline structure an energy input using a laser – in this case one tuned to 632 nm. The detected spectrum shows not only the reflected laser, but signals at other wavelengths. These peaks result when the natural vibration frequencies of the crystal efficiently absorb energy from the laser, leaving the reflected signal with less energy than the incoming one. Non pristine “defective” nanotubes absorb energy in a band around 0.164 eV. A JY-Horiba Raman with automated baseline correction is used for all spectra shown. D/G ratio is calculated through normalizing the integrated intensity of the G band and then measuring the integral of the D band signal.

Raman is an optical technique, and slight variations in the focus can allow the spectrometer to “penetrate” to varying depths. In all cases, the measurements were taken with the focus set for maximum intensity on the G-band signal using a 1/2 second exposure, followed by a full spectrum taken with a 15 second exposure. As the spot size of the laser is small compared to the sample size, two spectra are taken at random positions per sample. Only if both overlay well is the sample used in the data set.

Conductivity

Precise measurement of the electrical conductivity for a SWCNT ribbon sample is difficult – the measureable voltage drop is of the same order as metal wire, however standard samples are no larger than circular 12.5 mm punch. At these sizes, voltage

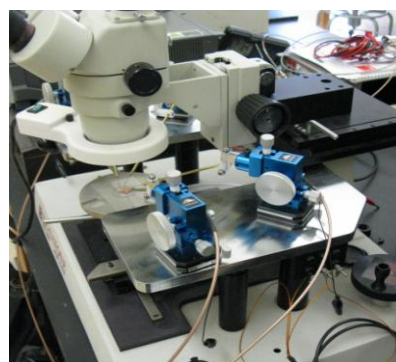


Figure 3 Conductivity Measurement

drop is on the order of microvolts, and it is desirable that the error in measurement be less than 5%. National Instruments digital multimeter and source/measure hardware is available for use, and sufficiently sensitive. Four point measurements are used to eliminate contact resistance from voltage measurements[20] – by using voltage-sense probes held at constant, zero current, the voltage can be measured probed without any worry of a voltage drop between the probe and the sample. The Van der Pauw method [21] shall be used for the determination of sheet resistances, combined with a thickness measurement to back out bulk conductivity. A dedicated punch shall be used to ensure that samples are of similar geometry, even though the method is supposed to be independent of geometric factors. This method of measurement involves reconfiguration of probe leads for each test as well as finding an iterative solution to the transcendental equation $V = V_0 \frac{1}{1 + \frac{r^2}{R_s^2}}$, making measurement of numerous samples a tedious and time consuming task[21, 22]. Additionally, the large degree of manual involvement in these measurements implies a reduction in precision and repeatability. A full electrical conductivity characterization solution is developed, including LabVIEW software integrated with a switching matrix, high resolution volt meter, and digital source unit, to perform these tasks in a consistent and reliable manner. Probes (shown in Figure 3) are placed around the periphery of a sample, current is passed through two sets of adjacent probes, and the voltage drop measured between the other two probes. The configuration of probes is shifted clockwise three times, giving four rounds of measurement and two different polarities. These IV sweeps are used to calculate four sheet resistances, the average of which is taken to be the sheet resistance of the sample. If differential between any two sets of IV sweeps is greater than 5 times the smallest sheet resistance, a flag is set informing the user to check their contact.

Error Analysis

The conductivity measurement setup was checked using high purity aluminum foil sourced for battery applications, and the conductivity of said foil was

measured in a stable manner at $35.8 \times 10^6 \text{ S/m}$, within 5% of the CRC handbook value of $37.6 \times 10^6 \text{ S/m}$. When measuring nanotube papers, the most egregious source of error is not only the thickness measurement, but the variation of thickness across the paper. Given that the thickness from a filtered paper varies $\sim \pm 5 \text{ }\mu\text{m}$, this variation can be on the order of 10%, however, the worst-case deviation would imply the entire paper is skewed, in which case it would no longer be variation, but a change in thickness. Repeated measurement of the same samples show spreads of approximately 10% - the aggregate measurement is primarily limited by clean voltage differentials, with lower conductivity, the less spread in the measurement. Given that the parameter of bulk conductivity is dependent on the absolute thickness, which is estimated to 6% accuracy. Of the approximate 10% error in absolute conductivity, most of it is due to the thickness parameter in converting from sheet resistance to bulk conductivity. While not of absolute concern to this work, an interesting workaround of this problem (which is most straightforwardly resolved by increasing uniformity of papers) is to use the often cited figure of merit "Specific Conductivity", conductivity / density. As conductivity is [thickness / sheet resistance] and density is [mass / (area*thickness)], the thickness terms cancel, allowing the figure of merit to be calculated using only the mass of a sample and the area of the 2D punch.

Tensile Strength

This work will include a pilot study in order to determine effective testing parameters that shall be used as a standard for all further mechanical testing. The bulk of this work shall be performed using NPRL's Q-800 (Figure 4), a tensile test device purchased from TA Instruments with a maximum travel of 24 mm, maximum applied force of 18 N, and a resolution of .001 N in force and 1 micron in length measurement.

While reflux-type nanotube ribbons have tensile strength on the order of 100 MPa, low density/high purity samples are known to have tensile strengths an order of magnitude less than this, where the high resolution is of great importance.



Figure 4 TA Q800 Dynamic Mechanical Analyzer

Additionally, this level of sensitivity allows the use of the device in alternate configurations, such as nanotube ribbons in bending. Should additional testing of samples requiring greater than 18 N of force be necessary, a larger Instron tensile tester is available from RIT's Mechanical Engineering department. This device has a 110 N load cell, however the data carries significant noise and there is a great deal less control of testing parameters.

A standard tensile test is performed by first clamping the material at a pressure of 21 MPa using smooth jaws. Initial length is measured under a .01 N load after the stage temperature reaches the desired level. Once thermal equilibrium has been reached, the DMA displaces the lower clamp at the desired rate, and monitors the force necessary to achieve the desired strain rate.

Error Analysis

As the Q800 generates a stress strain curve with a length resolution of 0.1 μm with a minimum sample length of 4.5 mm, the error in strain is negligible for purposes of these experiments. The stress measurement, however, is derived from a number of measurements, namely the thickness, width, and force. Error in thickness using the micrometer is limited to the tool's published accuracy of 3 μm , as well as thickness variations along the filtered paper. To minimize this error, each 8mm x 3mm tensile test strip has the thickness measured at 3 points along its length, and the smallest of these is used, as this is where stress will be highest during the test. A standard paper thickness is $\sim 50 \mu\text{m}$, giving an estimated error in thickness of 6%. Similar limits of error can be applied to the width, however, this is always at least 3 mm, and as such the error in width is limited to less than 0.5%. The force measurement, accurate to .05 N, results in an error in stress of $\sim .4 \text{ Mpa}$. While the magnitude of this force-induced error is large compared to small measurements that are possible, measurements that fall under the 2 Mpa threshold shall be assumed as "zero" for the purpose of this study. Measurements of interest fall in the 20+ Mpa range, and the error here is limited to the 6% from thickness.

Thickness measurement

Measuring the thickness of a SWCNT paper is extremely important when calculating engineering properties such as tensile strength and electrical conductivity. A common method used for accurate thickness measurement of materials in the lab is the electron microscope. A sample of the CNT paper is mounted in the Phillips X-90 ESEM and precisely tilted such that the sample is perpendicular to the detector. In this state, extremely accurate thickness measurements can be taken, as seen in the image below. Resolution with this method is better than 100 nm, making it the method of choice in the NPRL for quite some time. However, should one begin to question the uniformity of thickness across the whole material, rather than the edge, difficulties arise. A sample from the

center of a paper requires measuring a cut edge, and the method of cutting can influence the measurement.

A proposed solution to this problem is the digital micrometer. Commonly available with an accuracy of 3 microns, the resolution is significantly worse than the electron microscope. The benefits of using this method include much faster measurements and ability to measure the central portion of a nanotube paper, however but one must account for “crush” in the SWCNT ribbon during measurement. In order to validate thickness measurements and dependent calculated properties performed using micrometer thickness, this modulus must be determined. It is proposed that a stack of SWCNT papers of approximately 5000 μm will deform sufficiently under a large crushing force to produce the necessary data for this calculation. The experiment shall be performed using the Carver hydraulic press, making sure that the moving and fixed plates remain parallel for each measurement. Data can be collected at 1000 psi increments in the hydraulics; this will linearly correlate to much higher pressures in the nanotube stack. The elastic modulus will be measured for both NPRL reflux and commercially produced materials between 50 MPa and 1 GPa. It is expected that the material will behave elastically to a point, and that this elastic behavior can be extrapolated to the pressure applied by the clutched micrometer.

Chapter 4: Description of Research Problem

An obvious gap in published literature is the relationship between processing conditions, morphological attributes, and the physical properties of these SWCNT bulk materials. This is a major shortfall in the effort to construct strong, conductive wires and ribbons from SWCNTs. Through careful study of the purification and processing steps used to create ribbons from SWCNT soot, one can further understand how the morphological attributes of the ribbons affect bulk engineering properties; tensile strength, electrical conductivity, toughness. For example, a quick thermal oxidation at 550 C, 30 minutes at 460 C, or 60 minutes at 420 C can all be used to produce nanotubes of the same purity[1]; however bulk properties of tubes produced with the three different processes were not characterized. There are many mechanisms that nanotubes can burn, such as fuse-burning and cutting at specific sites[23]. As the rate of oxidation for amorphous carbon is expected to be linear with temperature by tweaking the time and temperature of the thermal oxidation step, one could attempt to preserve both the length and purity of the nanotube bulk, taking advantage of theory that the electrical conductivity and mechanical strength of the material are directly related to the average length of nanotubes[4]. This is but one example of an opportunity to increase the quality and improve the engineering properties of nanotube bulk materials with process refinement. An obstacle encountered when attempting to improve the bulk engineering properties of bulk carbon nanotube ribbons is that the baseline material must be well characterized. This data has drawn interest from numerous parties public and private; carbon nanotube wiring harnesses have been slated for a wide range of applications, from high-tech spacecraft and terrestrial data centers to a sustainable replacement for copper wiring in common residential housing. Properties such as flexure & fatigue, high frequency AC conductivity, performance in dry and humid environments, vacuum and high pressure, low temperatures and high temperatures, Additionally, it is unavoidable that the nanotubes will be forced to interface with metals at some

point, and characterization of this interface is also of importance for application of the technology[24].

Critical Parameters

It is important to identify critical parameters which control the properties of SWCNT materials. While literature has identified a number of properties which should affect the SWCNT conductivity and strength[6, 25], in this work the critical parameters shall be identified as density, impurity content, defect density and nanotube length. Thermal oxidation affects all of these parameters, and shall be studied in depth. Other processes that single out these parameters include filtration pressure (density, impurity content), sonication (length), vacuum annealing (defects) and addition of nanostructured carbon (impurity content). Additionally, experiments shall be performed to determine any temporary or permanent environmental effects of temperature and humidity on the conductivity of SWCNT papers

Proposed Solution

The goal of this work is to address many of these problems in part, with a strong focus on fundamental research for strength and conductivity in bulk nanotube materials. The bulk of research will be completed using SWCNTs synthesized in the Semiconductor and Microsystems Fabrication Laboratory at RIT. The first phase of this work is to research characterization techniques for determining the tensile strength and electrical conductivity of nanotube ribbons and wires. After techniques for these measurements have been solidly chosen, measurements on NPRL-produced reflux, NPRL-produced purified and commercially available SWCNT sheets will be taken to gain familiarity with the procedures and build statistically strong baseline numbers for the specific materials used in this work. The second phase of work is where changes to engineering properties and morphological attributes are studied. Specifically, select processes will be controlled during synthesis and the material changes characterized. Modifications to the synthesis and purification process specifically include acid

reflux, thermal oxidation, sonication, post-purification addition of amorphous carbon, and thermal vacuum annealing, processes which have previously been noticed to cause variability in final nanotube ribbons and more importantly, are often chosen arbitrarily. The third phase of work involves technology demonstrations of SWCNT ribbons and wires in DC and RF applications. Additionally, the effects of temperature, pressure, and humidity on the electrical properties of bulk SWCNT materials provide insight into fundamental conductive mechanisms in the material not well understood. It has also been shown that increasing the density of any particular sample of nanotubes increases the conductivity; however the necessary techniques to perform the experiment while controlling and measuring length do not yet exist. Many works of literature propose that as the length of individual nanotubes increases, so should the conductivity of the bulk mat [4, 16, 26]. This is not observed in experiment, as nanotube materials with advertised tube lengths ranging over 3 orders of magnitude show similar conductivity.

Chapter 5: Production of Carbon Nanotubes

All SWCNT material was produced using a laser vaporization technique. A target of graphite powder with 3% mass fraction of 2 μm nickel catalyst particles is prepared via 48 hours of mechanical mixing and subsequently pressed into a 1.125" puck placed in an 1150° C tube furnace under a 200 sccm flow of Argon at atmospheric pressure. A Nd:YAG laser at 1064 nm is rastered over the target and fired with a 10 Hz pulse rate; the resulting vapor condenses as SWCNTs on the tube

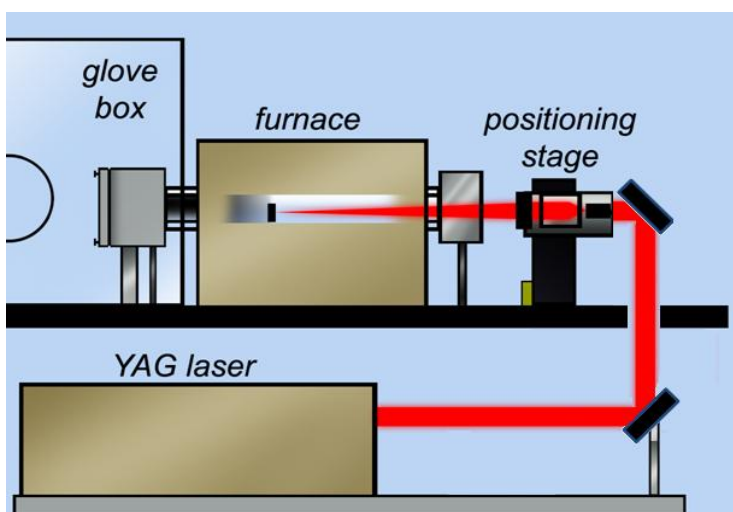


Figure 5 YAG Laser vaporization CNT synthesis

walls. An overview of the laser optics train is shown (Figure 5).

This material, as produced, contains large quantities of carbon impurities in addition to the nanotubes and metal catalyst particles. A standard procedure used to purify the soot is an acid

reflux, where the soot is boiled in

a 4:1:25 solution of 16M HNO_3 , 12M HCL , and deionized H_2O . This reflux is performed for 15 hours, after which the solution is removed using a 2 μm teflon filter, forming a paper of carbonaceous material. Filtration is followed by 6 alternating rinses of DI H_2O and Acetone, which further dissolves free carbon and reacts with leftover acids. The final product has approximately 2% metal oxide residue from the catalyst and 30% non-nanotube carbonaceous impurities. 60 psi air is used to press the paper onto the filter and evaporate any remaining acetone or water. The resulting papers from this process are considered the baseline material for the work presented – these initial steps of material production are not altered.

Chapter 6: Characterization of CNT Papers

Characterization of Mechanical Properties

The tensile strength of standard recipe SWCNT ribbons will be measured as a function of temperature. Baseline tensile strength characterization data shall be collected for synthesized nanotube material. NPRL – produced SWNT ribbons were subject to mechanical characterization, before and after acid reflux treatment. The non-reflux ribbons were purified to > 90% via a thermal oxidation treatment, while the reflux papers were produced using nanometal catalyst that provides >95% purity without the need for thermal oxidation. Both are formed to ribbons using vacuum filtration, and the final thickness of the paper is determined. In-house mechanical testing is performed using a TA Instruments Q800 Dynamic Mechanical Analyzer (DMA).

The tensile strength of reflux SWCNT ribbons is seen to have some dependence on both strain rate and temperature. At room temperature, the breaking strength was 180 MPa at 1.7% and at high temperatures the strength was 108 MPa at nearly 3% elongation. Data is shown in Figure 6. Tests were performed at a 15 Mpa / minute strain rate for consistency, though the dynamics of the nanoscale effects of strain rate on the strength of a mat of tubes is interesting. Other CNT material, purchased commercially, was also measured using the same procedure (Figure 7).

SWCNT papers show interesting properties when exposed to cyclic thermal loads under constant stress. The paper is mounted in the DMA fixture as per the tensile test procedures, however, the stress is ramped to a constant level of 7 Mpa and the position of the clamp monitored while the temperature is cycled. Cooling is

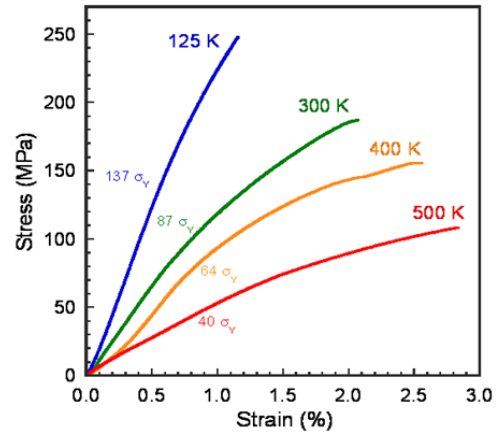


Figure 6 Tensile tests of Reflux material at varied temperature

accomplished by expanding LN2 in the test chamber, and heating via electric heating grids.

Of particular interest is the tests performed following thermal cycling – notably that the ribbons gain room-temperature strength following the treatment. The ribbons tested were cycled 5 times from 175 K to 575 K. All cases of thermally-cycled material show increases in strength, ranging from 10-30 percent over un-cycled material.

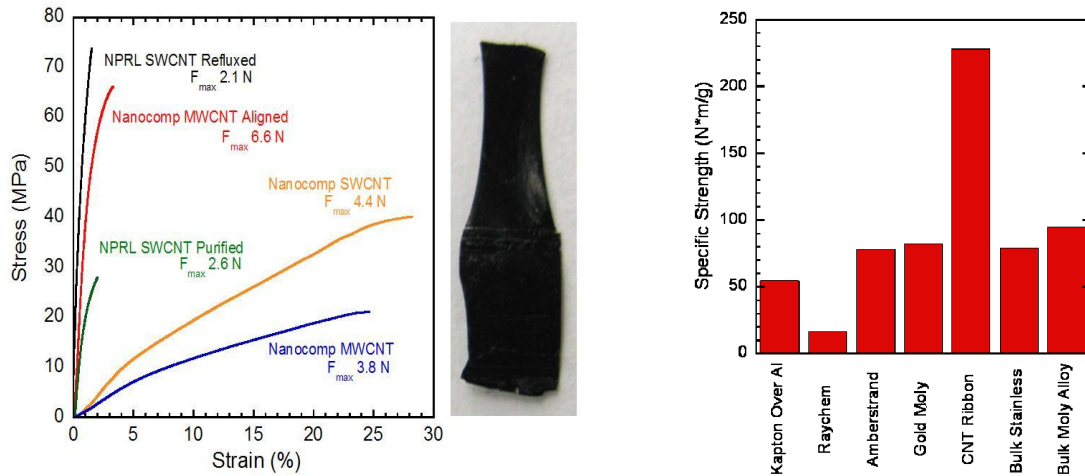


Figure 7: (Left) Tensile tests of CNT Materials (Right) Specific Tensile Strength of Materials

In general, SWCNT materials are observed to be somewhat variable in tensile strength – it appears that the manual filtration step lacks consistency needed for accurate characterization. An average reflux paper has a strength of 60-80 Mpa, however numerous exceptional specimens prepared in the same manner exhibit strength twice this range. Additionally, the NPRL produced material lacks the ductility of Nanocomp material, causing misaligned stresses to be concentrated and causing early failure. In comparison to metals the strength to weight ratio of nanotube papers is excellent and should not pose a limitation in the usage of SWCNTs as aerospace conductors.

Electrical Conductivity Data

Using methods described above, various nanotube materials are characterized for their electrical conductivity. Standard-preparation ribbons made from reflux material show a conductivity of 2×10^5 S/m, while after purification this drops by a factor of four, to 5×10^4 S/m. High-temperature vacuum anneals are observed not to provide any significant change in conductivity, but further processing with organic solvents such as hexane and xylene further reduce the conductivity by 2-3 fold.

Commercial material was acquired from Nanocomp, and the conductivity of this material was measured at 2.8×10^4 . Additional material from NanoIntegris was acquired and formed into papers, with a recorded conductivity of 2.3×10^4 S/m for

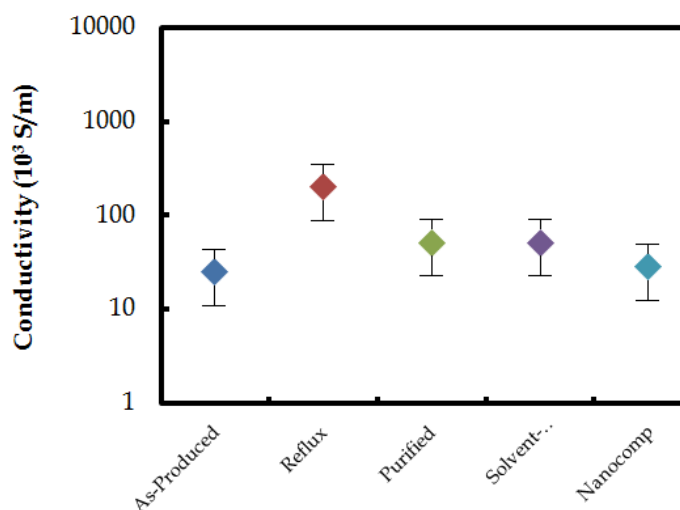


Figure 8 Conductivity of synthesized CNT Material

the metallic 99.9% type-pure nanotubes, and 1.8×10^4 S/m for the semiconducting (Figure 8).

In contrast, ongoing work at the Nanopower Research Labs for conductivity enhancement through chemical additives has recorded 2×10^6 S/m using a gold bromide dopant. The nitric acid used in an acid reflux provides a doping effect; the

application of organic solvents brings about a reduction in conductivity as the organic solvents react strongly with the acid, preventing it from performing as a dopant.

Chapter 7: Processing Modification

During nanotube synthesis, the production of nanotubes is accompanied by the growth of NC as well as amorphous carbon coatings around the nanotubes[27]. Thermal oxidation removes both kinds of carbon, leaving primarily nanotubes. This does not preclude the nanotubes from oxidizing, and evidence suggests that a standard oxidation removes at least 30% of the CNTs. However the addition of NC does not restore the electrical conductivity and mechanical strength that is lost during oxidation. This suggests that the carbon coatings found on nanotubes after laser synthesis contribute positively to both the mechanical and electrical properties. By varying processing parameters that affect the coatings, perhaps this can be proven.

Section 1 -Thermal Oxidation

Proposed Work

Baseline testing from Phase 1 shows that fully purified SWCNT material has inferior engineering properties to pre-oxidation reflux material; however the thermal oxidation is a necessary step to guarantee material consistency, remove any constituent amorphous and nanostructured carbons, and drive out excessive oxidizers that remain in the paper. It is proposed that a partial purification is necessary to optimize the properties of a SWCNT ribbon for conductive wire applications. It is possible to produce purified nanotubes using a variety of thermal oxidation recipes(Figure 9) [1]. The oxidation attributes of forms of carbon that occur in SWCNT vary and a

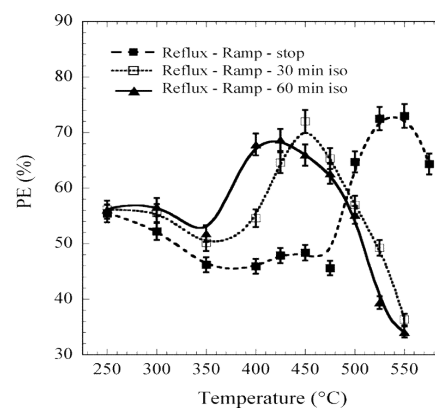


Figure 9: Purification Efficiency. From [1]

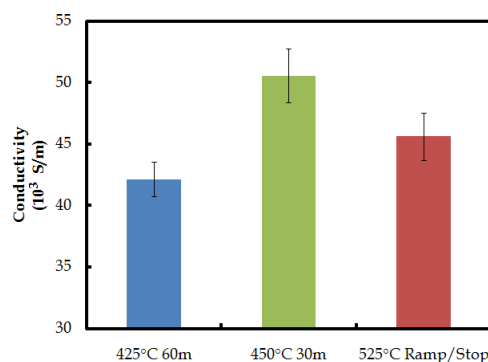


Figure 10 Conductivity of purified nanotubes using different oxidation recipes

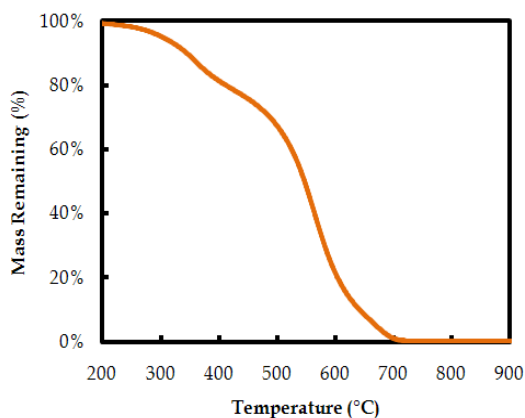


Figure 11: TGA Thermogram of SWCNT reflux material

TGA curve for NPRL reflux paper can be decomposed into constituents, including nanotubes, graphite, and NC (Figure 11). It is expected that the oxidation rates for these constituents do not vary equally with temperature. Figure 10 shows that reflux material subject to the three different purification efficiency peaks have quite different conductivity. Of particular

importance are the numerous shortening mechanisms dependent on oxidation, which have a strong dependence on temperature[28, 29]. While length of individual tubes of a bulk sample cannot be accurately measured, the bulk properties can be, potentially differentiating oxidation schemes that preserve CNT length in comparison to schemes that shorten the nanotubes. If bulk properties respond as described in theory, optimization of the thermal oxidation step for minimal tube cutting will be important in the production of strong, conductive CNT material.

It is proposed that samples of NPRL reflux material shall be burned in air at different temperatures, with samples removed from the furnace at different oxidation times. The tensile strength and electrical conductivity of these samples shall be measured, and further studies will be performed to generate data at points deemed of interest. Additionally, ramp-stop and ramp-isotherm data at a number of temperatures shall be taken using the TA Instruments Q5000 TGA for reflux and nanostructured carbon samples.

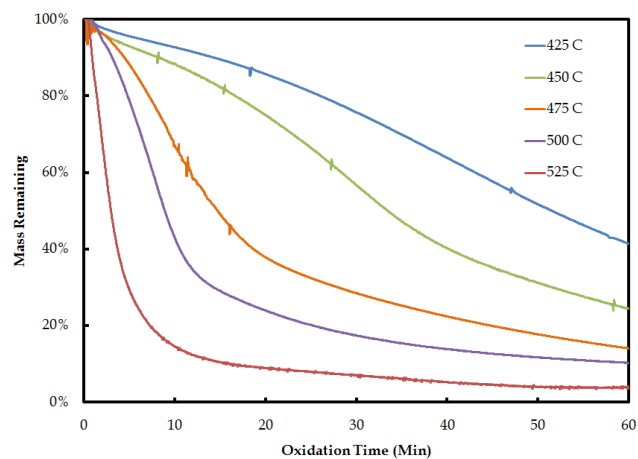


Figure 12 Isothermal Mass loss

Details

The purpose of this study is to estimate the magnitude of structural damage caused by standard SWCNT purification. Carbon nanotubes were produced using established laser-ablation techniques according to reported procedure with a pulsed Nd-YAG laser in a nitrogen atmosphere, followed by a 15 hour Nitric /HCl acid reflux to remove metal catalyst particles [8,9]. The resulting dispersion was filtered through and dried onto a 2 μm Teflon filter paper, resulting in a paper of $\sim 30\ \mu\text{m}$ thickness consisting of both nanostructured (NC) carbon and SWCNTs. Thermal oxidation is the standard method for removing the amorphous carbon from this material [7, 10], figure 5 shows the mass loss as a function of time. SWCNT paper was divided into 5 mm squares for this experiment. Each square was subject to isothermal TGA analysis, during which the mass-loss as a function of time is recorded. Each temperature is repeated twice. Figure 12 displays the mass loss as a function of time at various isothermal oxidation temperatures. The most notable feature of these curves is that they generally contain two slopes, an initial fast-burn followed by a slower oxidation. At all temperatures, the material ends up with 3-4% residual mass, though the figure is truncated at 60 minutes for clarity. The tensile strength and electrical conductivity of the material is measured at select points along this curve, representing a specific thermal oxidation treatment.

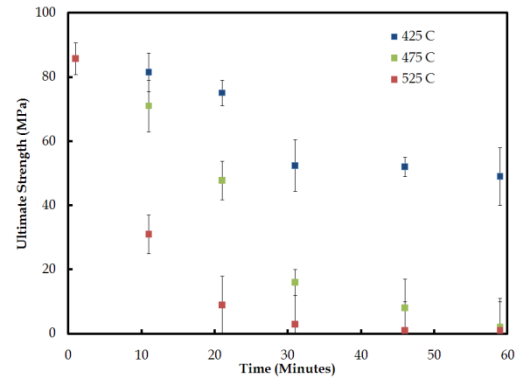


Figure 13: Tensile strength lost during purification

It has been observed that the thermal oxidation of amorphous carbon impurities at temperatures below the combustion point of carbon nanotubes has an oxidative effect on the nanotubes which is not accompanied by significant mass loss when observed using thermo gravimetric analysis. However, CNT papers held at these elevated temperatures in air display significant reductions in mechanical and

electrical properties, as shown in Figure 13 and Figure 14. It is possible that the nanotubes are undergoing shortening of some sort; however there is no technology able to quantify length with good statistical error available. AFM measurements are possible, though difficult, requiring relatively pure nanotubes. Observation of nanotube length in raw soot or acid refluxed CNT materials is unreliable; meanwhile statistics would require many more samples than possible.

SWCNT reflux papers were submitted to thermal oxidation in air for extended periods of time. The materials show a loss of mechanical strength,

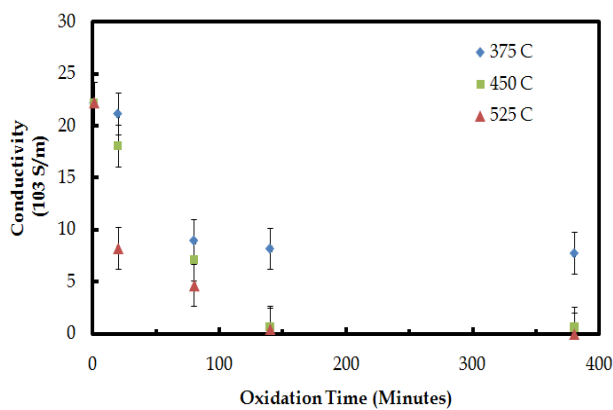


Figure 14 Conductivity loss during oxidative purification

occurring most rapidly in the first hour of oxidation, while changes in strength after three hours of oxidation are nearly zero. It was observed that ribbons oxidized at both 450°C and 525°C reached a final strength of < 3% of original, while those oxidized at 375°C maintained 25% of original tensile strength after 3 hours. From

these results, oxidation at temperatures ranging from 390 to 475°C for a duration less than one hour were identified to be of particular interest, as this is where the rate of change for paper tensile strength was greatest. During the first hour of oxidation at these temperatures, samples held at 425°C and below were observed to lose approximately 25% of original strength, while the sample burned at 475°C experienced a strength reduction of 95%. Of particular interest is that at 425°C, there is a significant mass loss after one hour when compared to the 390°C oxidation, yet strength remains similar. The conductivity remains longer than the tensile strength, though the remaining material is hardly cohesive and requires extreme care to measure.

Amorphous and nanostructured carbons are theorized to oxidize more quickly than pristine carbon nanotubes; however the presence of defects makes this somewhat ambiguous. The results suggest that either some fraction of non-nanotube carbon improves the physical strength of a SWCNT ribbon, or the oxidation is destroying nanotubes as well as impurities. As shown in literature, a coating of NC forms on the nanotubes during synthesis in addition to free carbon in the ribbon. The optimal thermal oxidation would remove discrete carbon, while leaving both nanotubes and NC coatings intact, preserving strength while removing unnecessary weight from the material. Of particular interest is that after 45 minutes at 425°C, the strength to weight ratio increased by approximately 10% of baseline.

Section 2: Nanostructured Carbon

Proposed Work

Non-nanotube carbon is primarily present in two forms; free amorphous carbon interdigitated with the nanotubes and conformal amorphous carbon coatings around the nanotubes. Assuming that these forms of carbon oxidize at roughly the same rate, the purification process is expected to remove them equally. However, the two forms of carbon have significant morphological differences, and as such are expected to have different contributions to the engineering properties of bulk SWCNT materials. As described, non-nanotube carbon can be produced in the same reactors used for SWCNT synthesis simply by omitting the catalyst. By adding this carbon to purified SWCNT papers, one can generate a bulk material lacking the conformal carbon coatings, however with the same mass-wise purity as the starting material. The variation in electrical conductivity and tensile strength will provide insight on the role of conformal amorphous carbon coatings on the bulk properties of SWCNT ribbons. It is expected that the addition of nanostructured carbon in this form will not contribute to the bulk properties of the material, rather as purity is reduced so should the bulk properties. In contrast, as the conformal coatings are

removed from a SWCNT paper, a marked reduction in mechanical strength is observed.

Mechanical testing of purity-controlled CNT reflux ribbons showed that nanometal ribbons with their amorphous carbon content reduced through thermal oxidation exhibit more strength when that carbon is not artificially replaced during processing. However, the greatest mechanical strength is observed when the as produced nanotube material is not subject to any oxidation following the acid-reflux.

This experiment shall involve NPRL reflux paper thermally oxidized to a purity of at least 95% and a sufficient quantity of nanostructured carbon. A constructed sample set will be produced where the NC is added to purified material. Sample purity verification via UV-Vis will be performed in addition to tensile strength and electrical conductivity. TEM and SEM microscopy could be used to show that the carbon is not conformal to SWCNT bundles but rather in large clumps.

Details/Results

The purity of a CNT sample was modified through the addition of nanostructured carbon (NC), a carbonaceous by-product of laser vaporization nanotube synthesis. All samples were prepared through the standard acid-reflux process following a thermal oxidation at 450 C for 30 minutes. Impurities are stirred into the material prior to filtration. By changing only the ratio of nanotubes to other carbon, it was observed that samples with the greatest mass fraction of CNT were also the most conductive.

Another result of the thermal oxidation is that nanostructured carbon is removed from the bulk CNT matrix. As the thermal oxidation purification is accompanied by a loss of mechanical strength and electrical conductivity, the possibility that the carbons within the matrix provide a strong bond was investigated. Nanostructured carbon was produced in the NPRL laser ablation reactors, making sure to prevent

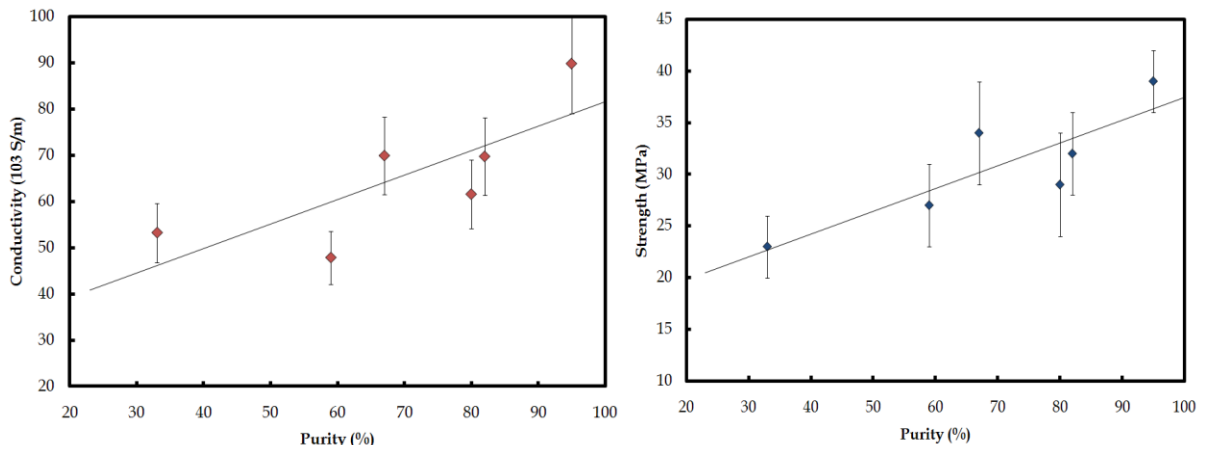


Figure 15: Addition of Nanostructured Carbon reduces Conductivity and tensile Strength

nanotube growth by omission of the catalyst. This additional carbon was added to the acid-reflux CNT slurry, dispersed in acetone and allowed to stir for 3 days before vacuum filtration. The resulting papers were seen to have reduced mechanical and electrical properties, while still forming a cohesive CNT paper (Figure 15). This provides contrast with an “as produced” paper, which generally do not form a cohesive mass with measurable tensile strength.

Even after dilution of the nanotubes 3:1 by weight, the papers retained approximately 50% of their tensile strength and electrical conductivity. The reduction appears to be linear with the addition of more carbon; however, there is a breaking point around 35% purity where the formation of a cohesive paper is rare due to the amount of carbon soot.

Nylon-SWCNT Paper Composite Materials

Polymers have been shown to coat and bond nanotubes to one another[30]. Addition of a polyamide was accomplished through the use of polymers soluble in solvent that also penetrate SWCNT mats with the goal of increasing mechanical strength[31, 32]. Specifically, the solution used for this process contained Scientific Polymer Products Nylon 6-3 [poly

(trimethyl hexamethylene terephthalamide)] dissolved in dimethylacetamide (DMA) at a concentration of 25 mg / ml; an ultrasonic bath maintained at 60°C was used to aid in dissolution. The nanotube material for this experiment was an acid-reflux SWCNT paper. The paper was fully submersed in the nylon-DMA solution for 5 seconds and dried at 120°C in air. Figure 16 shows that the adherant nylon coats the nanotubes as well as bridging small voids between nanotubes.

SWCNT ribbons briefly exposed to the nylon-DMA solution showed a significant (48%) increase in tensile strength, as well as fourfold increase in the elongation before break, while the elastic modulus fell to approximately half, from 3.6 to 1.5 Gpa (Figure 17). The composite material also showed a qualitative improvement in toughness, being significantly more resistant to puncture and tear than the original SWCNT ribbon. The mass increase after 4 hours of drying at 120°C was 14%, and the thickness of the ribbon increased from 71 to 84 microns.

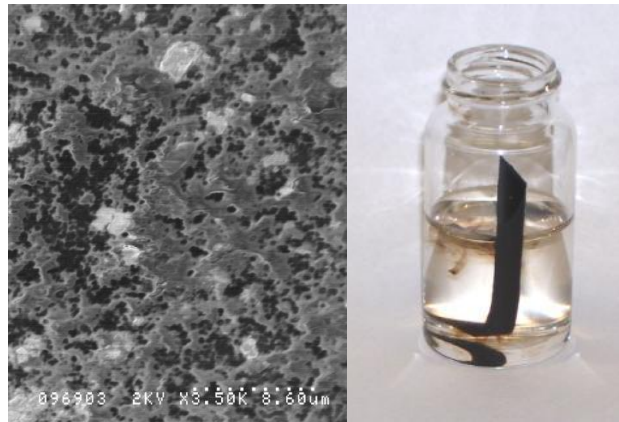


Figure 16: (Left) SEM Image of nylon CNT composite (Right) Nylon DMA solution penetrates CNT papers; solvent removes loosely-bound carbon

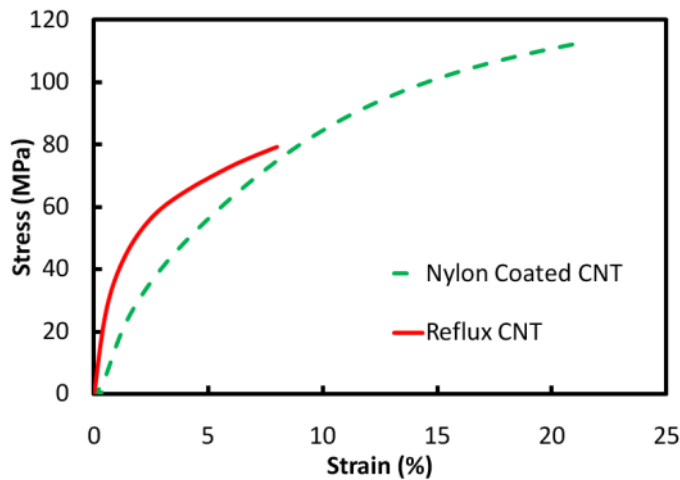


Figure 17: Tensile test of reflux CNT ribbon, before and after nylon treatment

reduction in tensile strength, permeating these voids with nylon appears to provide additional nanotube-nanotube or bundle-bundle bonding at the nanoscale, which improves the macroscopic mechanical properties of the ribbon as a whole. Of considerable interest is that the tensile strength of bulk Nylon 6-3 in is 90 MPa, while the original acid-reflux SWCNT ribbon had a tensile strength of 78 MPa; the resulting composite has a tensile strength greater than either constituent material.

The change in thickness is primarily due to swelling of the ribbon from intercalated nylon. After accounting for the changes in tensile strength, mass, and thickness, the strength-to-weight ratio of the composite increased by 51%. Just as removing carbon

impurities from void spaces between nanotubes causes a

Section 3: Vacuum Anneal

Proposed Work

As ribbons straight out of the reflux process are quite acid-heavy, they are reactive and not suitable for application without some sort of stabilization processing. One solution is the thermal oxidation, where high temperatures drive a majority of the acid from the SWCNT paper. However, should oxidation of the paper prove detrimental to improving the bulk properties, high temperature exposure in vacuum

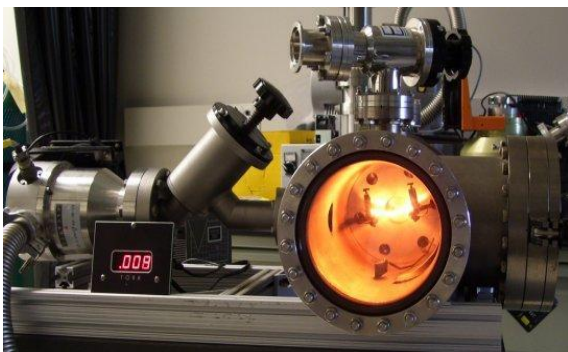


Figure 19: Vacuum Annealing Chamber

or inert gas may provide a method to drive out the acids without damaging the SWCNTs or causing graphitic transitions[33, 34]. Additionally, the annealing process has been shown to heal certain types of defects in a nanotube[35]. It is proposed that a sufficient anneal for these purposes will be 1 hour at a temperature determined through experiment. SWCNT papers subject to the annealing study shall have the mechanical and electrical properties measured post anneal before being subject to numerous thermal oxidation processes. It is expected that the vacuum anneal will provide the nanotubes a greater degree of resiliency to the thermal oxidation, and a harsher oxidation can be performed without significant degradation to the SWCNT properties. The challenge will be to settle

on an appropriate annealing time and temperature that prevents graphitic transitions from occurring, as there are currently no straightforward techniques for the removal of graphite from nanotubes.

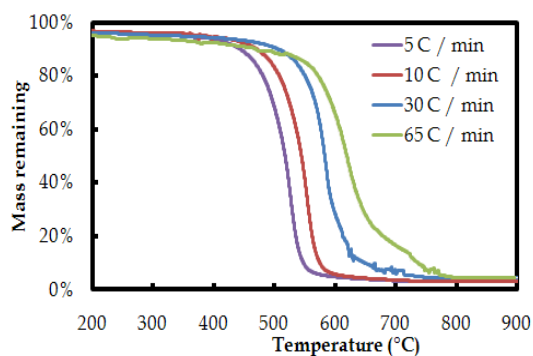


Figure 18: Thermogram of annealed SWCNT at various ramp rates

Details/Results

Post-anneal SEM imaging (Figure 20) shows that the anneal seems consolidate amorphous carbon into a form that appears similar to graphite, which was one major concern when beginning this work. However, as the thermogram of annealed SWCNT material shows complete combustion at temperatures as low as 525 C (Figure 18), the possibility of any graphitic transitions is negligible. An interesting trait that differ from otherwise equivalent CNT material is the lack of two separate

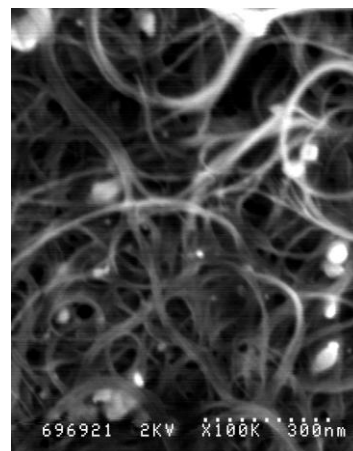


Figure 20 SEM of Annealed CNT Material

derivative peaks; there is only one broad peak, the position of which is highly ramp-rate dependent. In general the rate of oxidation is significantly less than non annealed material.

Given the importance of defects on the rate of thermal oxidation as seen when comparing TGA data to the D/G ratio (Figure 21), there is potential for vacuum annealing to stabilize the CNT paper and remove these defects without harming the paper.

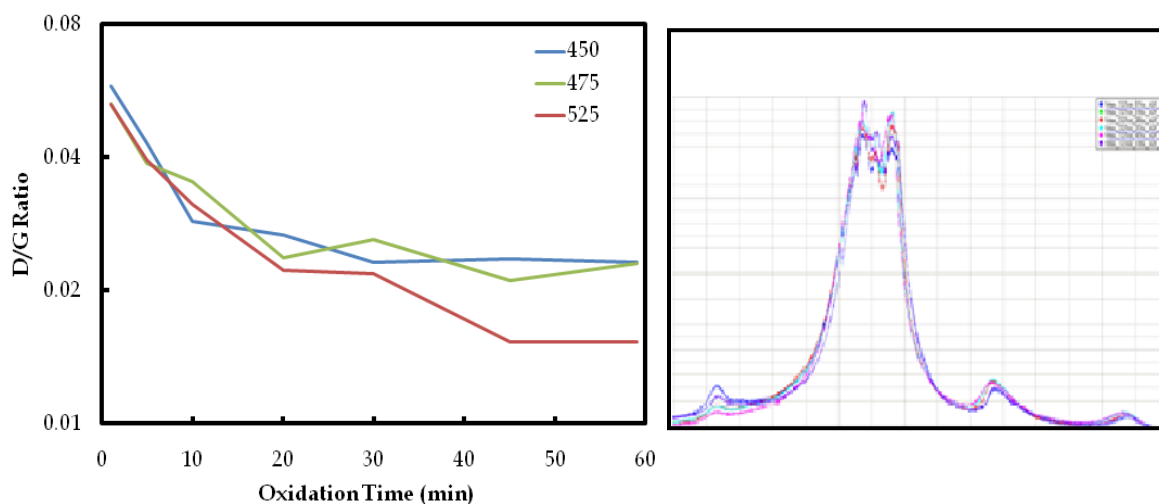


Figure 21 (Left) D/G ratio of post-anneal oxidation recipes (Right) Spectra for 475° C samples

The anneal was performed in 50° C increments from 700 to 900 °C. While the first 3 samples each show a reduced D band from the lower temperature, spectra for the

800-900 °C anneals overlay without distinction. As the elevated temperatures may have other unexpected side effects, the lower bound which still promotes maximum D/G ratio reduction

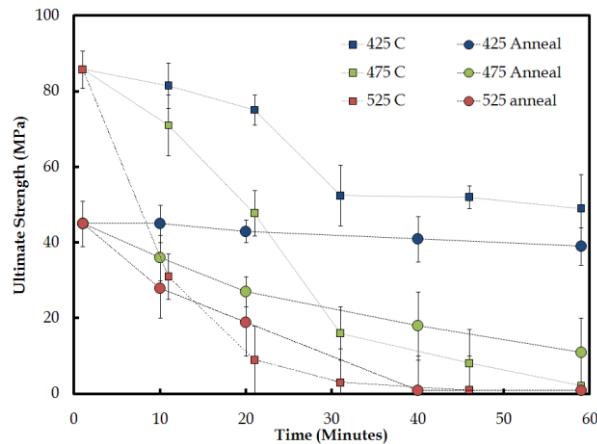


Figure 22: Tensile strength of CNT papers after isothermal oxidation

Raman characterization shows that, like other CNT material, the D/G ratio decreases with oxidation time, with oxidation rate correlated to but trailing the D band intensity.

Annealed material holds mechanical strength and conductivity better than reflux through the thermal oxidation process (Figure 22), though there is some

embrittlement imparted during the annealing process itself that causes poor initial performance. This embrittlement would make a vacuum-annealed reflux paper unsuitable for direct usage; however the process is of great interest going further as an intermediate step in the purification process. The excellent oxidation resistance of annealed nanotubes implies that the tubes are not being oxidized to the same degree as tubes in a standard reflux paper. Electrically, a HT annealed paper is unchanged from a vacuum-dried reflux paper.

Section 4: Analysis of thermal oxidation

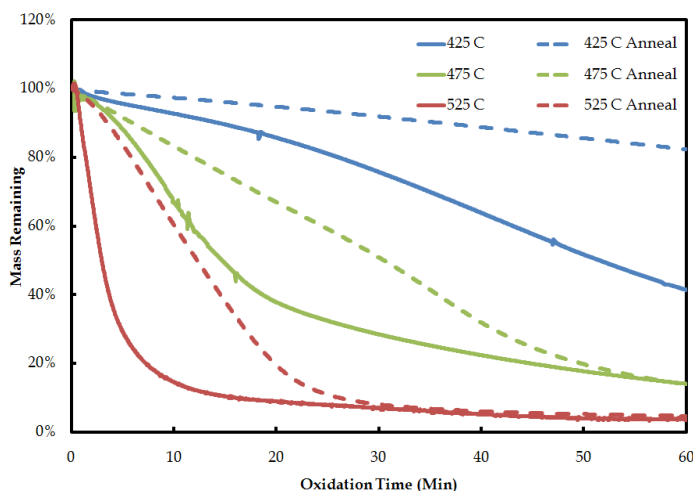


Figure 23 Comparison of isothermal TGA; Annealed vs Reflux SWCNT Ribbons.

One primary goal of this work is to develop an alternate thermal oxidation scheme based around the inclusion of the vacuum anneal. A useful metric for this endeavor is the logarithmic derivative, a relatively simple transform which allows one to convert the derivative of a “Percent remaining” TGA curve and

solve for the true oxidation rate in % per minute, *adjusting for the amount of mass remaining*. To do this, one would plot $-\frac{d(\ln(\text{Mass Remaining}))}{dt}$ rather than simply $-\frac{d(\text{Mass Remaining})}{dt}$. Elementary calculus shows that— $-\frac{d(\ln(\text{Mass Remaining}))}{dt} = -\frac{1}{\text{Mass Remaining}} \frac{d(\text{Mass Remaining})}{dt}$, thus accomplishing the goal by taking the natural logarithm of the percent remaining before taking the derivative. A downside of this method is clearly that when Mass Remaining and $\frac{d(\text{Mass Remaining})}{dt}$ are both small (near the end of the burn), there will be significant noise. As there are two primary constituent materials, it is expected that the logarithmic derivative plots will be decompose into two peaks – one representative of the nanostructured carbon and one representative of the nanotubes. If the anneal adds oxidation resistance to the nanotubes but not the NC, peak separation will increase after the annealing treatment.

Details

Isothermal TGA data comparing annealed and non-annealed SWCNT papers as they are oxidized at temperatures between 425° and 525° C is displayed in Figure 23. Clearly, the time it takes for the paper to completely oxidize has increased significantly. The peaks observed in annealed material (Figure 24) are a result of applying the logarithmic derivative to isothermal TGA. All contain similar

characteristics; right-skewed peaking functions with the peak heights increasing with temperature. It can also be observed that the degree of right-skew is temperature dependent, with less skew at higher temperatures and more at lower temperatures. The right skew is representative of two separate peaks, a smaller initial oxidation of the non-nanotube carbon followed by the oxidation of CNTs. By

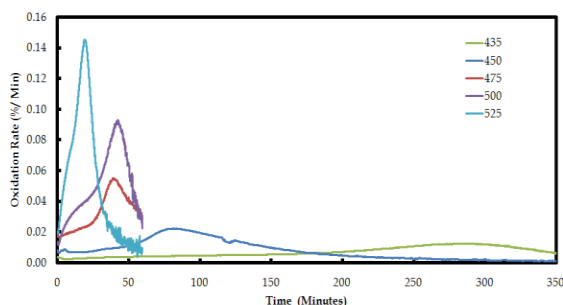


Figure 24 Logarithmic Derivatives, Annealed

using techniques similar to those in (Gupta), the decomposition into sub-peaks is straightforward. An example of this decomposition can be seen in Figure 25, where the combustion peak of the carbon is clearly separated from the nanotubes by approximately 45 minutes in the annealed material, but less than 15 minutes for the non-annealed material. Both isotherms were performed at 450° C. The NC peak shifts to the right and broadens slightly and nanotube peak shifts significantly more, while peak heights do not considerably change.

This behavior is representative of a sequential first-order reaction, where an intermediate transition is a prerequisite to mass loss. In this case, it appears that the intermediate product represents the decomposition of a sidewall defect into two nanotube ends[36]. As the total number of ends increase, the rate of mass loss follows; when there are no more defect sites remaining the rate slows down.

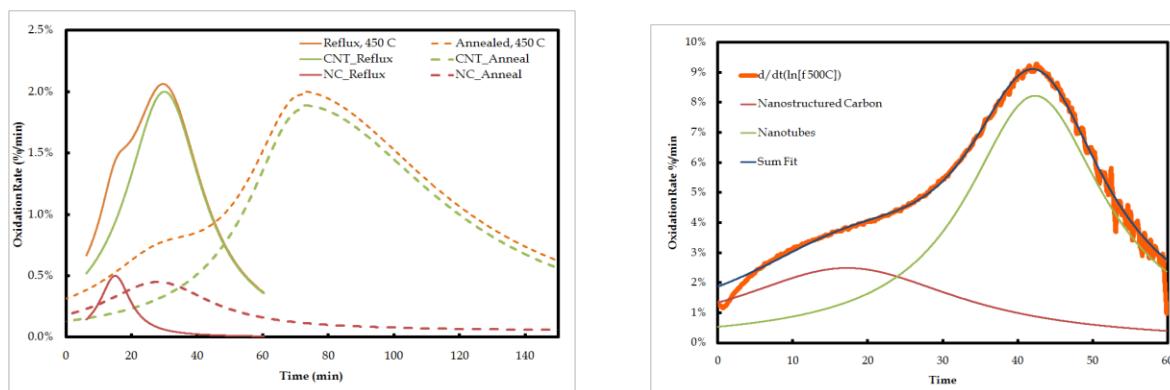


Figure 25: (Left) Comparison of 450° C Isotherm, Reflux vs Annealed. (Right) Curve-Fitting to TGA derivatives

Chapter 8: Environmental Effects

Section 1: In Situ Humidity Effects

It has been observed that the electrical conductivity of SWCNTs nanotubes have little response to temperature in vacuum. However, in the terrestrial environment, humidity is expected to play a significant role in the conductivity of a SWCNT wire, and when performing temperature-dependent properties in air the humidity level must be monitored.



Figure 26: ESPEC Environmental Chamber

Using an ESPEC terrestrial environmental chamber (Figure 26), NPRL and Nanocomp wires shall be subject to cyclical changing conditions including constant RH/changing temp, constant dew point, changing temp, constant temp/changing humidity, and changing temp/no humidity. Electrical conductivity shall be monitored using a 4 point method for the duration of these tests. To perform these measurements and control the environmental chamber, custom LABView software will be necessary. The use of a switching matrix will enable the testing of multiple samples at the same time. Both Constant -temperature / varied dew point, and constant dew point / varied temp shall be examined.

Humidity

It is well documented that SWCNT papers are quite hygroscopic, and the presence of moisture in their immediate environment will affect the conductivity. Much of this reactivity is due to defect sites, fundamentally

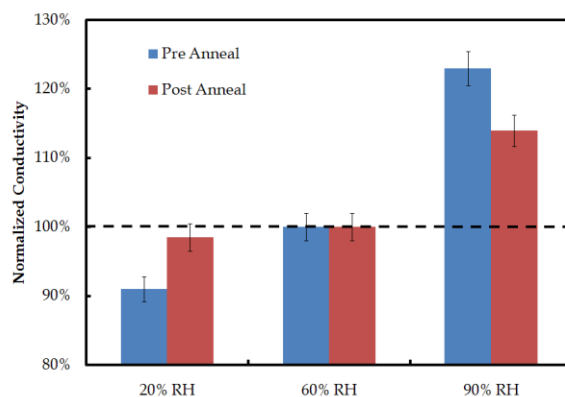


Figure 27: Annealing is shown to change the temperature dependence of CNT conductivity

studied in much CNT sensor work. It is expected that humidity reactions are related to D band intensity, as well as the presence of hygroscopic compounds in the bulk (leftover acid from the reflux, for example). A variety of nanotube materials were subject to thermal and humidity variations while the conductivity is monitored using a four-point measurement.

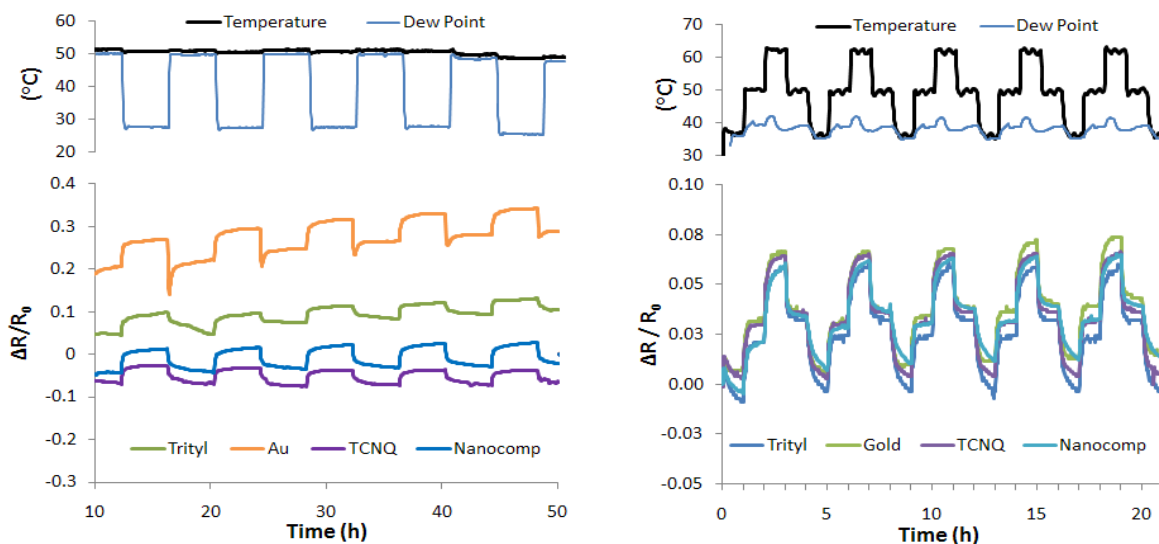


Figure 28: Humidity and Thermal Cycling of CNT Wires

Conditions ranged from <5% RH to 100% RH shall be studied, at temperatures from 5° C to 150° C, while stainless wire was used as a control, primarily for resistance to oxidation. Humidity was monitored using a Wet/dry bulb temperature using the NOAA “complex” form of the dew-point calculation. This option was chosen because of the wide variations in temperature and humidity, placing some of the more extreme points outside the range of the simple method. Clearly, as Figure 27 shows, there is a strong correlation of conductivity with humidity in the short term. Additionally, long term drift was observed for some materials with repeated cycling.

Temperature

Temperature was cycled with control of humidity, ranging from cycling with the chamber extremely dry, held at <10% RH at 90 C for 24 hours before beginning the test, as well as maintaining a constant dew point of 20 and 60 C. Additionally, very

high temperature measurements were performed with slight modifications to the vacuum annealing chamber for in-situ 4-point measurement.

It is seen that in a low humidity environment over a temperature range of 175 K, NPRL CNT papers undergo a 7-8 % swing in conductivity with positive correlation, while Nanocomp materials are about 3 times as sensitive, or 0.1 % / K. At a 20C dew point the temperature sensitivity does not change significantly, however in the presence of a constant 35 C dew point, the temperature sensitivity increases by ~ 120% (Figure 28). These results are preliminary however, as the environmental chamber used is not capable of maintaining a constant absolute humidity over wide temperature ranges and as such, the temperature range for constant dew point is only 50 K.

Section 2: Strain hardening, Flexure, Crush

Remarkably, SWCNT materials are shown to work harden yet at the same time have remarkable fatigue resistance. The work hardening properties of NPRL reflux material shall be studied, by first measuring the breaking strength, and subsequently pre-stressing the material to before re-testing the strength and elastic modulus. The plastic/elastic properties of SWCNTs are extremely important for processing, as material capable of withstanding moderate plastic deformation can be handled with traditional metalworking processes such as rolling and drawing. Additionally, SWCNT wires will be subject to high-cycle bend testing, using S.O.A spacecraft harness wiring as a comparison while the previously developed electrical testing scheme for multiple simultaneous four-point measurements will be applied.

Effect of Axial Pressure on Papers

NPRL-produced SWCNT material shows excellent resiliency to high pressure both mechanically and electrically. Standard acid-reflux purified material was used for the experiment, where conductive ribbons are placed between stainless steel dies with 1.125 inch diameter. A transparent

coating of Teflon is used to electrically insulate the nanotube ribbon from the die while hydraulics force the dies together with force varying from 0-100 kN, while electrical conductivity measurements are taken via the 4-point method to eliminate contact resistance from the calculation.

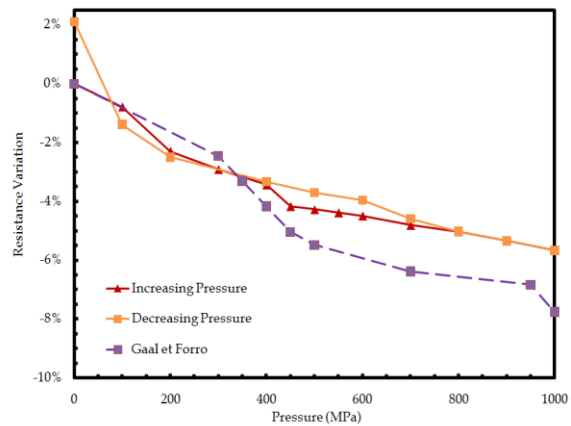


Figure 29: Decreasing resistance with pressure

Constant current is passed through the CNT ribbon using a Kiethley 2635 SMU. The voltage drop is measured before pressure is applied to the ribbon and modeled as two series resistors consisting of the ribbon not under compression and the ribbon under compression. The change in voltage drop is attributed only the

compressed section of ribbon. Figure 29 shows that as pressure is applied, a significant increase in the conductivity of the paper is measured. This effect has been measured previously by Gaal et Forro under hydrostatic pressure[x], with that data displayed for comparison. The SWCNT material did not appear deformed following the tests – Figure 30 shows CNT ribbons before and after the application of pressure.

The modulus of elasticity for this material is $1-2 \times 10^7$ Pascal, and Poisson's ratio is estimated at 0.1, allowing the calculation of the cross-sectional area as a function of pressure. Thus, the intrinsic property conductivity can be calculated as a function of the reduction in volume for a given mass of CNT paper, however, These results indicate that while densification plays a role in increasing the conductivity of these materials, alignment of individual and bundles of nanotubes during the densification process not only provides a better conductive pathway, but allows the material to retain in a densified state.



Figure 30 CNT Ribbon, before and after 1 GPA axial pressure

Bending

In exploration of the SWCNT wire's ability to withstand repeated flexure, two experiments were set up. The first involved repeatedly bending the wire using the TA instruments DMA. The force sensors were used to measure the resistance to bending; if this resistance drops suddenly, the wire has suffered some sort of structural failure. This test was performed on space-grade harness wire from TRW and Raychem as well

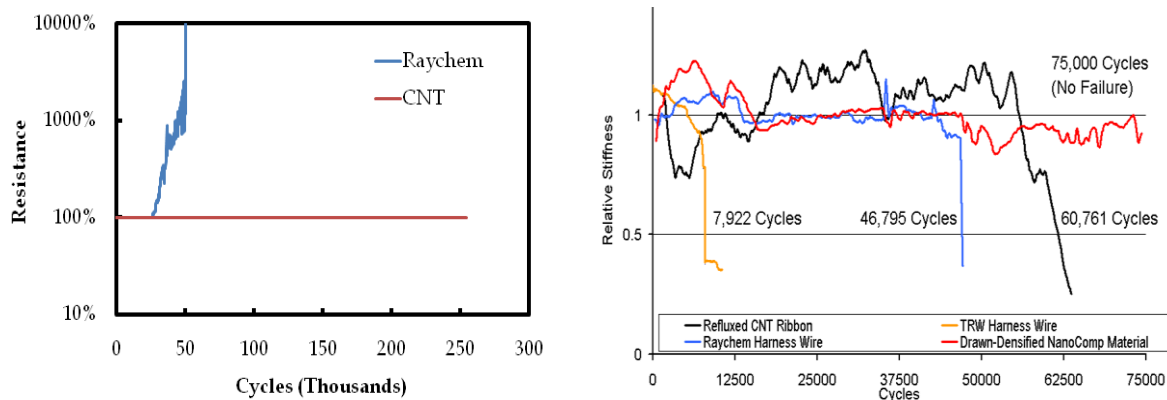


Figure 31: (Left) Electrical performance under bending (Right) Stiffness cyclic bending. (Below) Experimental Setup

as NPRL ribbons and drawn/densified wires produced from commercially available material. A similar test was also performed with the same setup, monitoring electrical conductivity instead of stiffness. These test (Figure 31) show that while NPRL CNT ribbons are susceptible to tearing, commercial materials appear to be unaffected. This is likely due to the greater elastic range of commercial material.



Strain Hardening

Repeat tensile testing on SWCNT ribbons shows a marked increase in breaking strength when the paper is pre-stressed. This was first noticed when a ribbon is placed in tension until failure and the remaining pieces are then tested – they

possess a higher yield and breaking stress as well as enhanced elongation at break. Additionally, a shift in elastic modulus is observed when a ribbon is pre-stressed. Figure 32 shows some example data of these effects. Electron microscopy (Figure 33) was used to search for evidence of alignment; however the only new features of

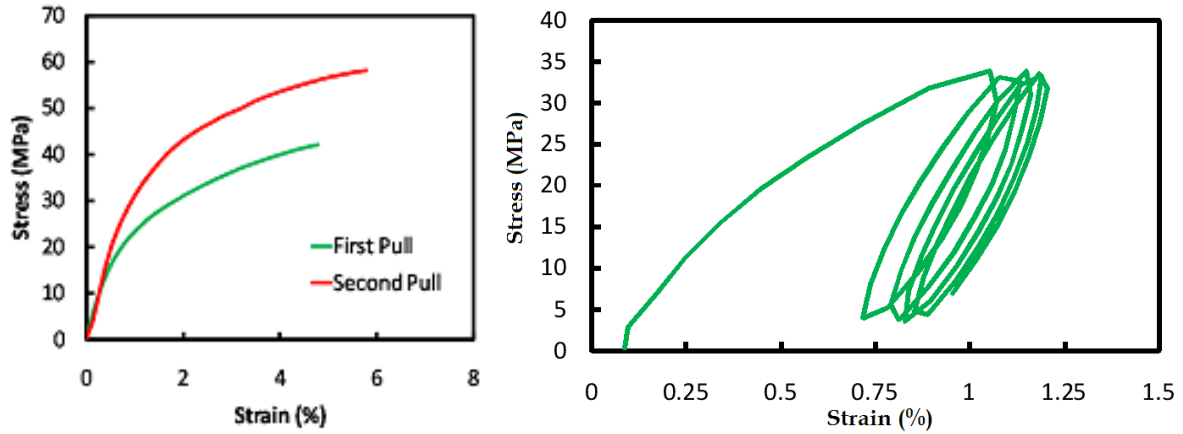


Figure 32 Strain Hardening of SWCNT Ribbons

significance are micron-scale creases, aligned with the direction of pull. Electrical conductivity was unaffected by whatever alignment is induced through the pre-stress process. It is remarkable that CNT papers undergo plastic deformation and work hardening similar to metals, while at the same time show nearly unlimited fatigue life.

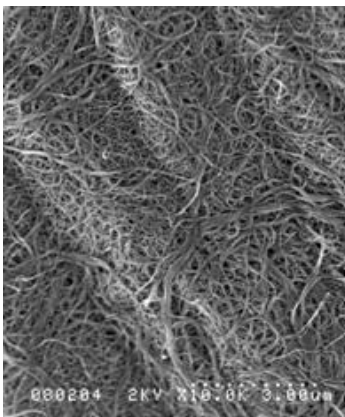


Figure 33: SEM Image of pre-stressed CNT Paper

Chapter 9: Discussion

In the previous section, the critical parameters for SWCNT bulk conductivity were identified as density, impurity content, defect density and nanotube length. The work focuses primarily on improving the production of strong, conductive nanotube materials through study of the thermal oxidation step, with minor forays into composites, addition of extra impurities, and physical reliability measurements.

Defects Caused via acid treatment

It is widely displayed in literature than the use of strong chemical oxidants cut nanotubes, leaving them shorter and broken up. A commonly chosen oxidant is Piranha solution, a

mixture of nitric acid and hydrogen peroxide.

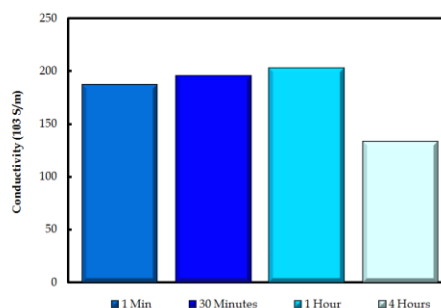


Figure 35: Conductivity and Piranha exposure

It appears that the induction of defects and chemical cutting through the use of acid solutions improves the conductivity of CNT materials when applied for a short time, but when treatment is too severe the conductivity drops again (Figure 35). It is difficult to compare acid-cut tubes to non-cut because of the strong doping effects present; however when exposed papers are compared to a specimen subject to one minute of exposure, the strong acids from the Piranha solution continue to increase conductivity, even though this acid causes significant shortening as demonstrated

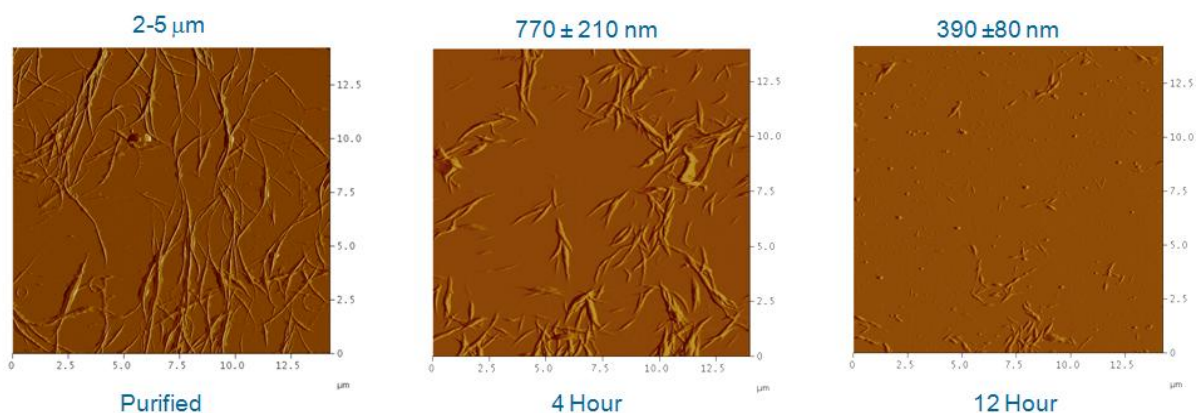


Figure 34: AFM Analysis of Piranha Oxidation; Courtesy of Dr. Brian Landi

both in literature and in the image sequence of Figure 34. Mechanically, acid-cut papers have virtually non-existent tensile strength or cohesion.

Removal of Defects during Oxidation

With the removal of the nanostructured carbons from the SWCNT bulk material, there is a marked reduction in the density, tensile strength and electrical conductivity of the paper. As seen in figures A and B, this reduction occurs in both pressure and vacuum filtration, though the reduction is less pronounced under pressure filtration. As seen in literature, it is known that thermal oxidation of nanotube materials not only oxidizes the amorphous carbons within the material, but also some of the nanotubes themselves. Investigation using Raman spectroscopy of samples subject to thermal oxidation shows a sharp reduction in the D band. It is evident that the rate of mass loss is related to the D/G ratio. D band resonance is generally caused by an imperfection in the axial symmetry of a nanotube, and when a defect is oxidized and a nanotube is cut, the D band response from that defect drops away. Thus, the defects in place following the standardized laser-ablation synthesis and acid-reflux purification are a catalyst for the oxidation of SWCNT carbon during the thermal oxidation.

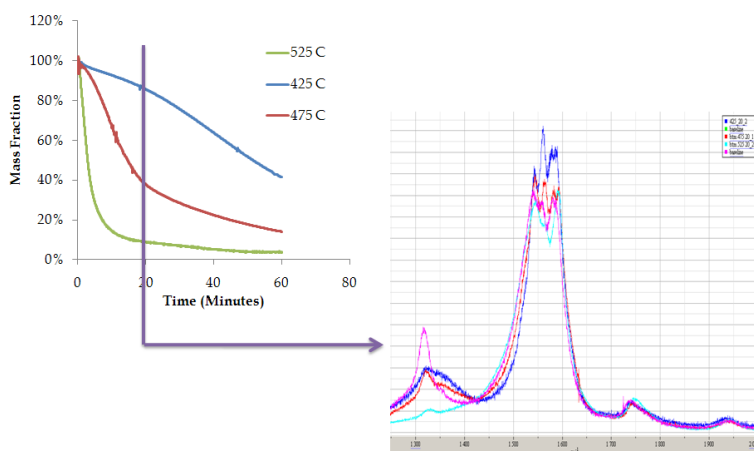


Figure 36: Initial D-Band (pink) reduces after 20 minutes of oxidation after thermal oxidation (Figure 36), providing evidence that if the oxidation does cause new defects, the rate is significantly less than the rate of decomposition at defect sites.

Chapter 10: Conclusion

The preceding work consisted of two distinct phases: in the first, methods of measurement were developed and evaluated, mechanical and electrical for various commercially available and synthesized nanotubes materials were characterized, and durability concerns such as work hardening, repeat bending, thermal effects, and humidity sensitivity were briefly evaluated. The second phase focused on possible improvements to the material for aerospace wiring harness applications, primarily consisting of an experimental study of purification process modifications. The initial measurements displayed the promise of carbon nanotube materials while building familiarity with the materials and processes involved. It was observed that present day carbon nanotube materials display favorable tensile strength-to-weight ratios when compared with metals. The elastic modulus increases with temperature, while the tensile strength is inversely related. Electrical conductivity of current materials, at 2×10^6 S/m, are approximately an order of magnitude too low to be of use in a current-carrying conductor, however data and low current applications could see significant weight savings. The electrical conductivity is weakly temperature dependent and quite sensitive to humidity, with the humidity dependence being linked to defect sites on the nanotubes. Also of note is that small changes in the purification process produce large changes in the properties of the nanotubes.

This observation sparked phase two of the work, an attempt to characterize the effects of processing changes on the material, with a focus primarily on the thermal treatments used to purify the material. This process in particular was chosen because of the marked reduction in strength and conductivity concurrent with removal of the non-nanotube carbons, while attempts to add nanostructured carbon back into the matrix showed only further reduction in properties. For comparison, the addition of Nylon at this step significantly improved mechanical strength. Additionally, a high-temperature vacuum anneal was studied due to the significant

effects it has on the thermal oxidation; the insertion of an 800° C, 1 hour anneal prior to the thermal oxidation cuts mass loss rates 3-4 times, clearly imparting a significant degree of oxidation resistance to the nanotubes. Raman spectroscopy was used to measure the D band resonant signal for nanotube materials throughout various stages of oxidation, and it was observed that the strength of this band loosely correlates with the derivative of mass loss, and a vacuum anneal significantly reduces the D band without mass loss. This provides insight that thermal oxidation of defects is the most significant factor in the oxidation of nanotubes – note that the goal of thermal oxidation is to remove non nanotube material, while taking advantage of the nanotubes thermal stability and low surface area to selectively combust carbon byproducts. Attempts to model the combustion of nanotubes as a sequential first-order reaction shows promise, where the intermediate reactant is assumed to be the conversion of defect sites into a new form prior to the actual mass loss.

While defect sites cause tubes to be more reactive in an oxidative environment, it was also observed that the removal of defect sites lessened sensitivity to humidity, though conductivity under standard conditions does not change with the anneal. The conductivity of SWCNT materials is quite intricately connected to the number of defect sites; they not only affect the thermal oxidation but the tubes ability to interact with other compounds (such as water vapor) in the environment, and chemical dopants are currently the method of choice for conductivity improvement. While the vacuum anneal may aid production of more pristine nanotubes, further work is necessary to increase the bulk conductivity

References

1. Landi, B.J., et al., *Thermal Oxidation Profiling of Single-Walled Carbon Nanotubes*. Chemistry of Materials, 2005. **17**(26): p. 6819-6834.
2. Skákalová, V., *Electronic transport in carbon nanotubes: From individual nanotubes to thin and thick networks*. Physical Review B, 2006. **74**(085403).
3. Shiraishi, M., *Conduction mechanisms in single-walled carbon nanotubes*. Synthetic Metals, 2002. **128**(235).
4. Hecht, *Conductivity scaling with bundle length and diameter in single walled carbon nanotube networks*. Applied Physics Letters, 2006. **89**.
5. Kodama, *Field-effect modulation of contact resistance between carbon nanotubes*. Applied Physics Letters, 2007. **91**.
6. Behnam, *Effects of nanotube alignment and measurement direction on percolation resistivity in single-walled carbon nanotube films*. Journal of Applied Physics, 2007. **102**.
7. Liu, *Dynamic elastic modulus of single-walled carbon nanotubes in different thermal environments*. Physics Letters A, 2007. **365**.
8. Shim, Liu, *Highly Dense and Perfectly Aligned Single-Walled Carbon Nanotubes Fabricated by Diamond Wire Drawing Dies*. Nano Letters, 2008. **8**.
9. Landi, B. and R. Raffaele, *Effects of Carrier Gas Dynamics on Single Wall Carbon Nanotube Chiral Distributions during Laser Vaporization Synthesis*. J.Nanosci. Nanotechnol., 2007. **7**(883-890).
10. Lei, *Selective Growth of Well-Aligned Semiconducting Single-Walled Carbon Nanotubes*. Nano Letters, 2009.
11. Popov., V., *Carbon nanotubes: properties and application*. Mater. Sci. Eng. R. , 2004. **43**: p. 61-102.
12. Landi, B., et al., *Purity Assessment of Single-Wall Carbon Nanotubes, Using Optical Absorption Spectroscopy*. J. Phys. Chem. B., 2004. **108**: p. 17089-17095.
13. Teo, K.B.K., et al., *Uniform patterned growth of carbon nanotubes without surface carbon*. Applied Physics Letters, 2003. **79**: p. 1534.
14. Schauerman, C., et al., *Impact of nanometal catalysts on the laser vaporization synthesis of single wall carbon nanotubes*. Carbon, 2009. **47**: p. 2431-2435.
15. Honjie, D., *Conductivity of Individual Carbon Nanotubes*. Science, 1996. **272**: p. 532-526.
16. Behnam, *Computational study of geometry-dependent resistivity scaling in single-walled carbon nanotube films*. Physical Review B, 2007. **75**.
17. Lee, R.S., et al., *Conductivity enhancement in single-walled carbon nanotube bundles doped with K and Br*. Nature, 1997. **388**: p. 255-257.
18. Dresselhaus, M.S., G. Dresselhaus, and M. Hofmann, *The big picture of Raman scattering in carbon nanotubes*. Vibrational Spectroscopy, 2007. **45**(2): p. 71-81.
19. Jorio, A., et al., *Characterizing carbon nanotube samples with resonance Raman scattering*. New J. Phys., 2003. **5**: p. 139.
20. Kiethley, *Low Level Measurements Handbook*. 6th ed. 2004, Cleveland, Ohio.
21. VanDerPauw, L.J., *A Method of measuring specific resistivity and hall effect coefficients of discs of arbitrary shape*. Phillips Research Reports, 1958. **13**: p. 1-9.
22. VanDerPauw, L.J., *A method of measuring the resistivity and Hall coefficient on lamellae of arbitrary shape*. Philips Technical Review, 1958. **20**: p. 220-224.
23. Lu, X., et al., *Scanning electron microscopy study of carbon nanotubes heated at high temperatures in air*. Journal of Applied Physics, 1999. **86**: p. 186.
24. Liu, Z., et al., *Benchmarking of Metal-to-Carbon Nanotube Side Contact Resistance*. IEEE Xplore, 2008. **987-1-4244-1911-1**.
25. Kaiser, *Modelling conduction in carbon nanotube networks with different thickness, chemical treatment and irradiation*. Physica E, 2008. **40**.
26. Nirmalraj, P.N., et al., *Electrical Connectivity in Single-Walled Carbon Nanotube Networks*. Nano Letters, 2009. **9**: p. 3890-3895.

27. Cassell, A.M., et al., *Large Scale CVD Synthesis of Single-Walled Carbon Nanotubes*. The Journal of Physical Chemistry B, 1999. **103**(31): p. 6484-6492.
28. Forrest, G.A. and A.J. Alexander, *A Model for the Dependence of Carbon Nanotube Length on Acid Oxidation Time*. The Journal of Physical Chemistry C, 2007. **111**(29): p. 10792-10798.
29. Boul, P.J., et al., *Reversible sidewall functionalization of buckytubes*. Chemical Physics Letters, 1999. **310**(3-4): p. 367-372.
30. Zhang, W., et al., *Polymers and Carbon Nanotubes*. Macromolecules, 2004. **37**: p. 256-259.
31. Gao, J., et al., *Nylon Nanotube Composites*. J. Am. Chem. Soc., 2006. **128**: p. 7492-7496.
32. B. Shim, J.Z., K. Critchley and N. Kotov., *Carbon Nanotube Composites*. Am. Chem. Soc. Nano, 2009. **3**: p. 1711-1722.
33. Kowalska, E., et al., *Influence of high vacuum annealing treatment on some properties of carbon nanotubes*. Journal of Thermal Analysis and Calorimetry, 2006. **86**: p. 115-119.
34. Kosaka, M., et al., *Annealing effect on carbon nanotubes. An ESR study*. Chemical Physics Letters, 1995. **233**(1-2): p. 47-51.
35. Tsai, J.T.H. and A.A. Tseng, *Defect reduction of multi-walled carbon nanotubes by rapid vacuum arc annealing*. Journal of Experimental Nanoscience, 2009. **4**(1): p. 87 - 93.
36. Bom, D., et al., *Thermogravimetric Analysis of the Oxidation of Multiwalled Carbon Nanotubes Evidence for the Role of Defect Sites in Carbon Nanotube Chemistry*. Nano Letters, 2002. **2**(6): p. 615-619.
37. Bae, *Supercapacitors Using Single-Walled Carbon Nanotube Electrodes*. Adv. Mater., 2001. **13**: p. 497.
38. Beckyarova, *Electronic Properties of Single-Walled Carbon Nanotube Networks*. J. Am. Chem. Soc., 2005. **127**: p. 5990.
39. Gaa'l, R., *Pressure dependence of the resistivity of single-wall carbon nanotube ropes*. Physical Review B, 2000. **61**(11).
40. Geng, *Effect of Acid Treatment on Carbon Nanotube-Based Flexible Transparent Conducting Films*. J. Am. Chem. Soc., 2007. **129**: p. 7758.
41. Gong, *The effect of high-temperature annealing on the structure and electrical properties of well-aligned carbon nanotubes*. Materials Research Bulletin, 2007. **42**: p. 474.
42. Ishii, *Resistivity reduction of boron-doped multiwalled carbon nanotubes synthesized from a methanol solution containing boric acid*. Applied Physics Letters, 2008. **92**: p. 202116.
43. Kaiser, V.S., *Electronic transport in carbon nanotubes: From individual nanotubes to thin and thick networks*. Physical Review B, 2006. **74**(085403).
44. Kang, *Micelle-Encapsulated Carbon Nanotubes: A Route to Nanotube Composites*. J. Am. Chem. Soc., 2003. **125**: p. 5650.
45. Kim, G., et al, *Magnetoresistance of an entangled single-wall carbon-nanotube network*. Phys. Rev. B, 1998. **58**: p. 16064.
46. Petit, *Temperature dependent resistivity of single wall carbon nanotubes*. Europhys. Letters, 1998. **41**: p. 683.
47. Skákalová, V., *Effect of Chemical Treatment on Electrical Conductivity, Infrared Absorption, and Raman Spectra of Single-Walled Carbon Nanotubes*. Journal of Physical Chemistry B, 2005. **109**(15): p. 7174.
48. Skákalová, V., *Effect of SOCl₂ Treatment on Electrical and Mechanical Properties of Single-Wall Carbon Nanotube Networks*. J. Am. Chem. Soc., 2005. **127**: p. 5125.
49. Skákalová, V., *Electrical and mechanical properties of nanocomposites of single wall carbon nanotubes with PMMA*. Synthetic Metals, 2005. **152**: p. 349.

50. Skákalová, V., *Raman spectroscopy of single-wall carbon nanotubes and graphite*. Journal of Applied Physics, 2005. 98: p. 24311.
51. Skákalová, V., *Ion irradiation effects on conduction in single-wall carbon nanotube networks*. Applied Physics A, 2008. 90: p. 597.
52. Sreekumar, *Single-Wall Carbon Nanotube Films*. Chem. Mater., 2003. 15: p. 175.
53. Wei, *Electrical transport in pure and boron-doped carbon nanotubes*. Applied Physics Letters, 1999. 74.
54. Wei, *Fabrication of aluminum-carbon nanotube composites and their electrical properties*. Carbon, 1999. 37: p. 855.
55. Whitten, *The role of free radical condensates in the production of carbon nanotubes during the hydrocarbon CVD process*. Carbon, 2006. 44: p. 1653.
56. Xu, *Magnetic barriers in graphene nanoribbons: Theoretical study of transport properties*. Physical Review B, 2008. 77.
57. Zhang, e.L., *Electrical and thermal properties of carbon nanotube bulk materials: Experimental studies for the 328–958 K temperature range*. Physical Review B, 2007. 75.

Appendix 1: Technology Demonstrations

In order to incorporate CNT papers into devices, at some point there needs to be electrical contact to metal conductors. A simple experiment was developed where the contact resistance of CNT material to metals can be measured as a function of applied pressure. It was observed that contact resistance to copper and zinc is low and nearly independent of pressure, while aluminum and stainless steel required more pressure and had more contact resistance (Figure 37).

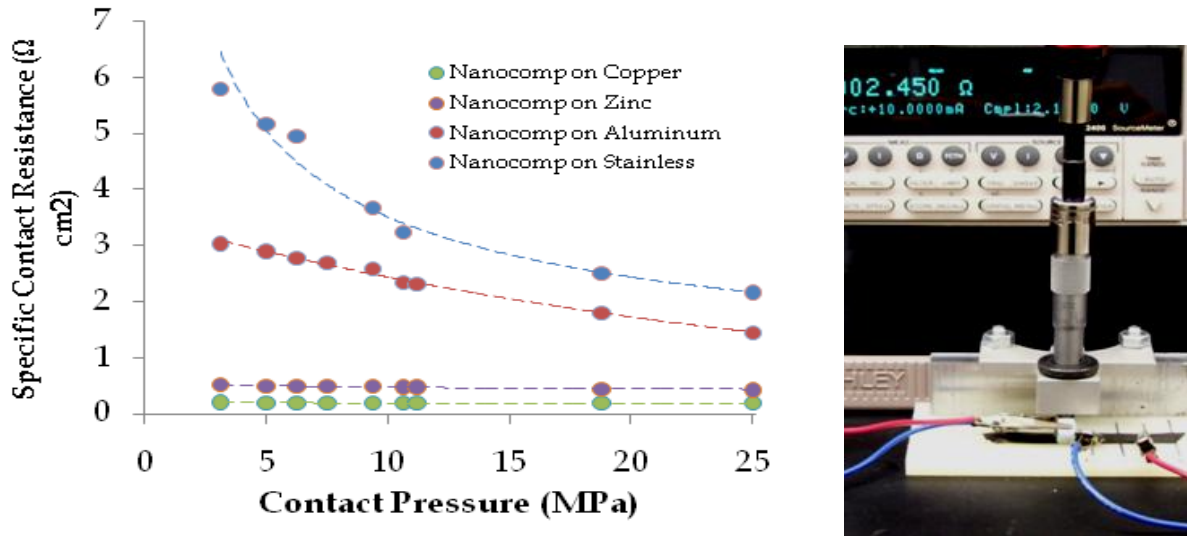


Figure 37 (Left) Contact Resistance of CNTs on Metal (Right) Contact resistance measurement setup

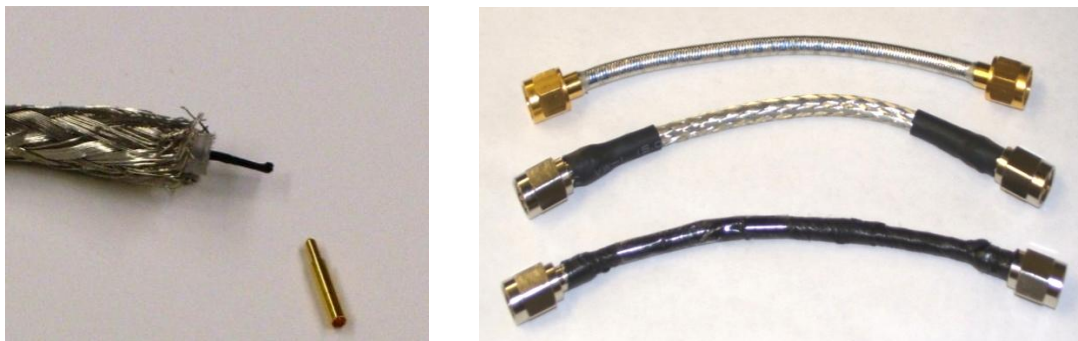


Figure 38 (Left) Coaxial cable with CNT center. (Right) Commercial SMA, CNT Center SMA, and CNT Shielded SMA cables.

Given low contact resistance to copper, it was apparent that for data transfer, a nanotube conductor could be used in their current state. A CNT SMA coaxial cable and an ethernet cable were produced (Figure 38). Additionally, the metal shielding of the CNT coax was replaced with nanotube ribbon.



Figure 39 (Above) CNT Ethernet Cable (Below) CNT ribbon bonded to photovoltaic



Though little detailed analysis was performed, the CNT coax allowed an Agilent network analyzer to function without difficulty, while the cable mass (not counting connectors) was 23% that of traditional RG-58 SMA cable it replaced.

The ethernet cable, while difficult to construct due to the connector, performed to Cat 5 standards and functioned at a 100 mbps transfer rate.

Additionally, CNT ribbon was also successfully used to contact a solar cell via silver epoxy (Figure 39). This particular application has garnered a great deal of interest from the aerospace community.

Appendix 2: DC Measurement Station

Given the importance of making fast and accurate DC measurements of CNT materials, a DC measurement system was developed using off-the-shelf parts and

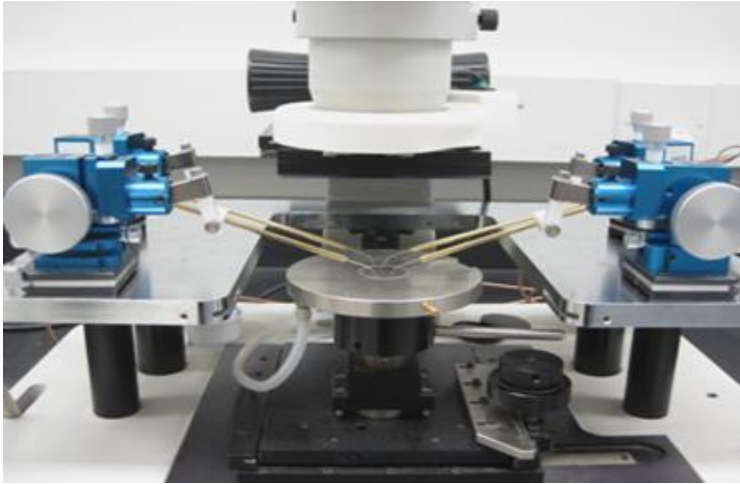


Figure 40 DC Conductivity Measurement Station

custom LabVIEW code. The system is based around National Instruments PXI hardware, the three primary components being a PXI-4130 high-precision source-measure unit, coupled with a PXI-4071 digital multimeter. The PXI-2503 switching matrix is also used for configuration of probe-instrument connections via software. On the physical end, a Cascade Microtech

probe station is used with tungsten needle probes, fine-adjust probe positioners, and a 10x optical microscope.

The standard procedure for making a Van der Pauw measurement begins with punching the CNT sample into an appropriate shape. A custom punch is used to repeatedly make the cloverleaf pattern. Using the microscope and hand positioners, the probes are placed as near as possible to the edge of the sample before executing the measurement program. The program then takes IV sweeps in all possible configurations of the probes by reconfiguring the switch, notifies the user of any contact problems, and calculates the sheet and bulk resistance using the VDP equation and the user-input material thickness. By raising and lowering the stage, numerous samples can be processed by simply placing each successive sample in the same spot on a glass slide; while the switching matrix and software remove any need to manually reconfigure connectors or perform iterative calculations in a separate excel spreadsheet. This setup replaced an Agilent B1500 on loan with a significantly faster and more convenient solution at less than 20% the cost.

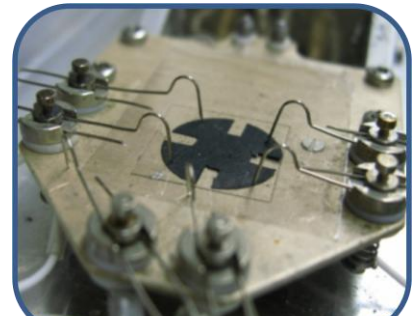


Figure 41 Van der Pauw Sample

